JOURNAL OF GEOPHYSICAL RESEARCH, VOL. 106, NO. D23, PAGES 32,481–32,501, DECEMBER 16, 2001

Large-scale air mass characteristics observed over the remote tropical Pacific Ocean during March–April 1999: Results from PEM-Tropics B field experiment

Edward V. Browell,[1] Marta A. Fenn,[2] Carolyn F. Butler,[2] William B. Grant,[1] Syed Ismail,[1] Richard A. Ferrare,[1] Susan A. Kooi,[2] Vincent G. Brackett,[2] Marian B. Clayton,[2] Melody A. Avery,[1] John D. W. Barrick,[1] Henry E. Fuelberg,[3] Joseph C. Maloney,[3] Reginald E. Newell,[4] Yong Zhu,[4] Michael J. Mahoney,[5] Bruce E. Anderson,[1] Donald R. Blake,[6] William H. Brune,[7] Brian G. Heikes,[8] Glen W. Sachse,[1] Hanwant B. Singh,[9] and Robert W. Talbot[10]

Abstract. Eighteen long-range flights over the Pacific Ocean between 38°S to 20°N and 166°E to 90°W were made by the NASA DC-8 aircraft during the NASA Pacific Exploratory Mission (PEM) Tropics B conducted from March 6 to April 18, 1999. Two lidar systems were flown on the DC-8 to remotely measure vertical profiles of ozone (O_3), water vapor (H_2O), aerosols, and clouds from near the surface to the upper troposphere along their flight track. In situ measurements of a wide range of gases and aerosols were made on the DC-8 for comprehensive characterization of the air and for correlation with the lidar remote measurements. The transition from northeasterly flow of Northern Hemispheric (NH) air on the northern side of the Intertropical Convergence Zone (ITCZ) to generally easterly flow of Southern Hemispheric (SH) air south of the ITCZ was accompanied by a significant decrease in O_3, carbon monoxide, hydrocarbons, and aerosols and an increase in H_2O. Trajectory analyses indicate that air north of the ITCZ came from Asia and/or the United States, while the air south of the ITCZ had a long residence time over the Pacific, perhaps originating over South America several weeks earlier. Air south of the South Pacific Convergence Zone (SPCZ) came rapidly from the west originating over Australia or Africa. This air had enhanced O_3 and aerosols and an associated decrease in H_2O. Average latitudinal and longitudinal distributions of O_3 and H_2O were constructed from the remote and in situ O_3 and H_2O data, and these distributions are compared with results from PEM-Tropics A conducted in August–October 1996. During PEM-Tropics B, low O_3 air was found in the SH across the entire Pacific Basin at low latitudes. This was in strong contrast to the photochemically enhanced O_3 levels found across the central and eastern Pacific low latitudes during PEM-Tropics A. Nine air mass types were identified for PEM-Tropics B based on their O_3, aerosols, clouds, and potential vorticity characteristics. The data from each flight were binned by altitude according to air mass type, and these results showed the relative observational frequency of the different air masses as a function of altitude in seven regions over the Pacific. The average chemical composition of the major air mass types was determined from in situ measurements in the NH and SH, and these results provided insight into the origin, lifetime, and chemistry of the air in these regions.

1. Introduction

The NASA Pacific Exploratory Mission (PEM) Tropics B (PTB) was conducted from March 6 to April 18, 1999 (DC-8 portion of PTB) to investigate the atmospheric chemistry of the remote tropical Pacific during the austral late summer to early fall [*Raper et al*., this issue]. This was the second in the series of NASA field experiments conducted in this region with the first (PEM-Tropics A (PTA)) conducted from August 30 to October 5, 1996 (DC-8 portion of PTA) [*Hoell et al*., 1999].

[1]Atmospheric Sciences, NASA Langley Research Center, Hampton, Virginia.
[2]Science Applications International Corporation, Hampton, Virginia.
[3]Department of Meteorology, Florida State University, Tallahassee, Florida.
[4]Department of Earth, Atmospheric, and Planetary Sciences, Massachusetts Institute of Technology, Cambridge, Massachusetts.

Paper number 2001JD900001.
0148-0227/01/2001JD900001$09.00

[5]Jet Propulsion Laboratory, California Institute of Technology, Pasadena, California.
[6]Department of Chemistry, University of California, Irvine, California.
[7]Department of Meteorology, Pennsylvania State University, University Park, Pennsylvania.
[8]Graduate School of Oceanography, University of Rhode Island, Narragansett, Rhode Island.
[9]NASA Ames Research Center, Moffett Field, California.
[10]Institute for the Study of Earth, Oceans, and Space, University of New Hampshire, Durham, New Hampshire.

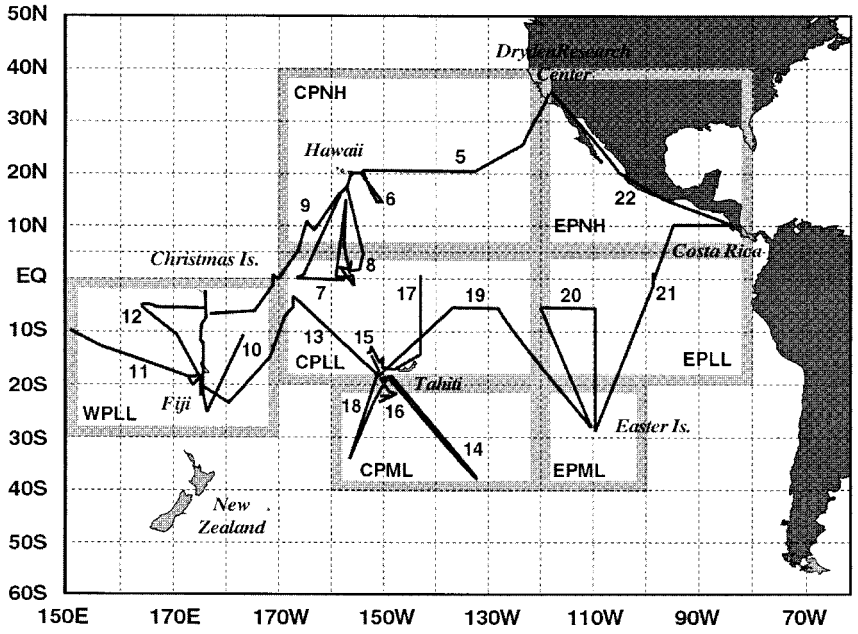

Figure 1. Map of PEM-Tropics B DC-8 flight tracks from February 19 to April 18, 1999, with flight numbers marked and regions used in air mass characterization investigations: central Pacific Northern Hemisphere (CPNH), eastern Pacific Northern Hemisphere (EPNH), western Pacific low latitude (WPLL), central Pacific low latitude (CPLL), eastern Pacific low latitude (EPLL), central Pacific midlatitude (CPML), and eastern Pacific midlatitude (EPML).

During PTB both the NASA Langley airborne UV differential absorption lidar (DIAL) and Lidar Atmospheric Sensing Experiment (LASE) systems were operated from the NASA DC-8 aircraft in nadir and zenith modes to collectively measure vertical profiles of ozone (O_3), water vapor (H_2O), aerosols, and clouds from near the surface to the upper troposphere along the aircraft flight track. In situ measurements of O_3 and H_2O were also made on the DC-8 to augment the lidar remote measurements. The flight tracks of the DC-8 during PTB are shown in Figure 1. A discussion of the PTB science objectives and the characteristics of the instrumentation on the DC-8 and P-3 aircraft are given in the overview paper by *Raper et al*. [this issue].

Eighteen DC-8 flights were made during the PTB field experiment with bases in Hawaii, Fiji, Tahiti, and Easter Island. Local flights were performed from these locations, and long-range survey flights were conducted between these bases and on the outbound flight from the NASA Dryden Flight Research Center at Edwards Air Force Base, California, to Hawaii and on the return flight from Easter Island to Dryden with a stop in Costa Rica. Details about the flight objectives and the specifics of each flight are given in the overview paper [*Raper et al*., this issue]. The survey flights of the DC-8 consisted mainly of en route ascents and descents with short, typically less than 20 min, constant altitude legs at specific altitudes of interest that were identified using the remote sensing real-time lidar data. This allowed for extensive vertical sampling of the troposphere along the flight track. On local flights the general strategy was to use the lidars to survey the troposphere along the flight track and to select the geographic regions and altitudes of interest for in situ airborne sampling. This approach allowed for the real-time synergistic use of data from the various sensors on the DC-8 to maximize the efficiency of the sampling strategy. This paper briefly reviews characteristics of the UV DIAL and LASE systems, discusses results from the PTB mission, and compares these results with those from the PTA mission conducted during the biomass burning season over this same region.

2. Instrumentation and Methodology

The current airborne UV DIAL system has been described in detail in several recent publications [*Richter et al*., 1997; *Browell et al*., 1998]. This system uses two 30-Hz, frequency-doubled Nd:YAG lasers to sequentially pump two dye lasers that are frequency-doubled into the UV to produce the on-line (288.2 nm) and off-line (299.6 nm) wavelengths for the DIAL O_3 measurements during PTB. The residual 1064-nm and ~590-nm beams from the frequency-doubling process of the Nd:YAG and dye lasers, respectively, are also transmitted with the UV DIAL wavelengths. As a result, four laser beams are transmitted simultaneously into the atmosphere below (288.2, 299.6, 576.4, and 1064 nm) and above (288.2, 299.6, 599.2, and 1064 nm) the aircraft for lidar measurements of O_3, aerosols, and clouds from near the surface to about 3 km above the tropopause. This system and its predecessor have been used extensively in airborne investigations of tropospheric and stratospheric processes over the last 20 years [see, e.g., *Browell*, 1983, 1989; *Browell et al*., 1998], including several NASA Global Tropospheric Experiments over the Pacific Ocean: Pacific Exploratory Mission (PEM) West A [*Browell et al*., 1996a]; PEM-West B [*Fenn et al*., 1997]; and PEM-Tropics A (PTA) [*Fenn et al*., 1999].

The UV DIAL system has an absolute accuracy for O_3 measurements of better than 10% or 2 parts per billion by volume (ppbv) and a measurement precision of 5% or 1 ppbv

with a vertical resolution of 300 m and an averaging time of 5 min (about 70-km horizontal resolution at DC-8 ground speeds) [*Browell*, 1983; *Browell et al*., 1983, 1985]. Intercomparisons between in situ and UV DIAL O_3 measurements are made throughout the course of a field experiment to insure the accuracy of the measurements is being maintained [see, e.g., *Fenn et al*., 1999].

The LASE system was initially designed for and operated from the NASA high-altitude ER-2 aircraft [*Browell and Ismail*, 1995; *Browell et al*., 1997; *Moore et al*., 1997]. This system uses a Ti:sapphire laser that is pumped by a double-pulsed, frequency-doubled Nd:YAG to produce laser pulses in the 815-nm absorption band of H_2O. The wavelength of the Ti: sapphire laser is controlled by injection seeding with a diode laser that is frequency-locked to a H_2O line using an absorption cell. Each pulse pair consists of an on-line and off-line wavelength for the H_2O DIAL measurements. The LASE system was operated for the first time from the NASA DC-8 during the 1998 Convection and Moisture Experiment (CAMEX 3), which was conducted to study hurricane characteristics with a large ensemble of airborne instruments [*Ferrare et al*., 1999; *Browell et al*., 2000]. During CAMEX 3, LASE was configured to simultaneously measure H_2O, aerosols, and clouds below and above the DC-8 using a back-to-back transmitter-receiver arrangement similar to that used for the UV DIAL system. This enabled LASE measurements to be made from near the surface into the upper troposphere.

The accuracy of LASE H_2O profile measurements was shown to be better than 6% or 0.01 g kg^{-1}, whichever is greater, in a major validation experiment conducted during 1995 [*Browell et al*., 1997]. During this experiment, two validation aircraft (C-130 and Lear jet) were used to provide in situ H_2O measurements along the LASE flight track, and one also had a H_2O DIAL system for remote measurements along the same path. In addition, special radiosonde balloons were launched, and a ground-based Raman lidar was operated for H_2O comparisons with LASE. Intercomparisons were also conducted in 1996 during the Tropospheric Aerosol Radiative Forcing Observational Experiment (TARFOX) field experiment [*Ferrare et al*., 2000a, 2000b]. Once the LASE system was configured for operation from the DC-8 in the simultaneous nadir and zenith modes of operation, additional comparisons were made with other sensors to insure the accuracy of the H_2O measurements. *Ferrare et al*. [1999] and *Browell et al*. [2000] discuss these intercomparisons in the context of CAMEX 3. The results were consistent with the initial LASE validation experiments.

An example of comparisons between LASE nadir and zenith H_2O profile measurements and in situ H_2O measurements from three different H_2O sensors on the DC-8 and a locally launched radiosonde is shown in Plate 1. Although the sampling between the various sensors is very different, there is good agreement between measurements. The greatest disagreement occurs in the two-stage chilled mirror hygrometer measurements at H_2O levels below 2 g kg^{-1} during ascent where the instrument is constrained by its maximum thermoelectric cooling capacity. The radiosonde launched from Tahiti generally agrees with the other measurements with the largest deviation in the midtroposphere of ~0.15 g kg^{-1}. After the cryogenic and diode laser hygrometer measurements were smoothed to the same 500 m vertical resolution of the LASE measurements, they showed excellent agreement with each other and with the LASE measurements. This further demonstrates the measurement capability of LASE across a wide range of H_2O concentrations.

Since the UV DIAL remote O_3 profiles begin about 750 m above and below the aircraft, the ozone distribution across this region is estimated by interpolating between the nadir and zenith UV DIAL measurements with the in situ O_3 measurement used to constrain the interpolation in between. Ozone distributions were also extrapolated from the lowest UV DIAL measurement altitude (usually below 1 km) to the surface using the gradient in ozone concentrations determined from the in situ measurements. These techniques were previously discussed for the UV DIAL O_3 distributions from the PTA field experiment [*Fenn et al*., 1999]. An example of the resulting O_3 distribution is shown in Plate 2 for the flight from NASA Dryden to Hawaii (flight 5). The aerosol scattering ratio distribution derived from the UV DIAL measurements on the same flight is also shown in Plate 2. The aerosol scattering ratio is the ratio of the amount of backscattered laser light from aerosols alone to the amount of backscattered laser light that would be expected from a clean (aerosol free) molecular atmosphere. The relative IR (1064 nm) lidar backscatter distribution, which represents scattering from aerosols and molecules, is normalized to a region that is estimated to be relatively clean (less than 2% of scattering attributed to contribution from aerosols), thereby yielding the total atmospheric scattering ratio. In this calculation the relative molecular backscattering distribution is determined from the remote atmospheric pressure and temperature measurements of the Jet Propulsion Laboratory (JPL) Microwave Temperature Profiler (MTP) along the flight track or from a meteorological analysis if the MTP data are not available. The aerosol scattering ratio is then just the total atmospheric scattering ratio minus one. Note that there is no attempt to correct for aerosol and cloud attenuation in these distributions.

Ten-day back trajectories for air parcels at 500 mbar along the flight track are also shown in Plate 2. These back trajectories were calculated using the Florida State University (FSU) kinematic back trajectory model. Air parcels along the flight track are selected at specific pressure altitudes, and these air parcels are followed back to their origins 10 days earlier (unless the trajectory terminates early at the surface). The consistency of the trajectories can be tested by using an ensemble of air parcels. This is discussed in detail by *Fuelberg et al*. [this issue]. The back trajectories shown in this paper are used to describe the general characteristics of the air mass' source region.

3. Results and Discussion

3.1. Air Masses Observed Over Pacific

A major air mass transition was observed during the survey flight from California to Hawaii on March 6, 1999 (flight 5). Plate 2 shows the O_3 and aerosol distributions observed along the flight track as well as 10-day back trajectories arriving at 500 mbar along the flight track. The air off the coast of California had significant levels of O_3 and enhanced aerosol loading across the entire troposphere. This situation gradually changed on the southwest flight leg such that the enhanced aerosol loading was no longer present and O_3 levels near the surface were observed to be in the low 20 ppbv level. Cirrus clouds were seen with tops as high as 12 km which was just under the tropopause. A stratospheric intrusion was observed on the westbound leg with O_3 levels over 60 ppbv extending

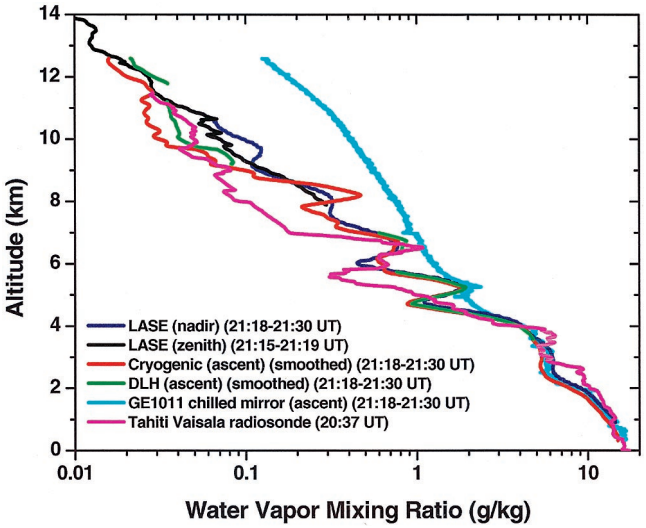

Plate 1. Water vapor profile comparisons between LASE nadir and zenith remote measurements and in situ measurements from the Buck CR-1 cryogenic hygrometer, NASA Langley Diode Laser Hygrometer (DLH), and GE-1011 chilled mirror hygrometer on the DC-8 and the Tahiti Vaisala radiosonde on local flight from Tahiti on April 2, 1999 (flight 15).

down to 8 km at 20°N. This intrusion modified the O_3 levels in the midtroposphere while O_3 below 2 km was in the 20–40 ppbv range. The 10-day back trajectory analysis for air parcels arriving at 500 mbar (~5.6 km altitude) shows that the air closest to the California coast probably originated over Asia. The origin of the air along the track changed to coming from the southwest and then the west with less aerosols and O_3 associated with it. This was a clear transition from a continental source to more of a marine background condition with the additional influence of the stratospheric intrusion.

A large contrast was found between the characteristics of air masses in the NH and SH across the Intertropical Convergence Zone (ITCZ). The meteorological conditions associated with PTB are described by *Fuelberg et al.* [this issue]. During PTB one segment of the ITCZ was located north of the equator between about 3° and 10°N. Plate 3 shows the O_3, H_2O, and aerosol distributions across the ITCZ on the flight from Hawaii to Fiji on March 17–18, 1999 (flight 9). The transition from NH air to SH air can be seen near 2300 UT in the abrupt O_3 decrease near the surface from 20–30 to less than 10 ppbv and in the midtroposphere from 40–60 to 20–40 ppbv. This decrease in O_3 was anticorrelated with the change in H_2O which generally increased everywhere below about 7 km. Convective outflow from upwind cloud activity can be readily seen in the H_2O data between 2130 and 2230 UT at an altitude of 6.5 km. The depth of the marine boundary layer also increased into the SH air. There is some evidence of a slight enhancement in aerosols in the NH air (see aerosol layer at ~4 km near 2130 UT). Cirrus clouds can be seen under the tropopause with the height of the tropopause increasing along the flight track from ~13 km in the NH to over 15 km south of the equator. A series of trajectories arriving at three pressure levels (850, 500, 200 mbar) along this flight track are given in Plate 4. In the middle and lower troposphere north of about 10°N, the flow of the NH air was predominantly from Asia, while the flow to the south was entirely easterly near the surface and variable in the midtroposphere with light winds and long residence times over the Pacific. In the NH upper troposphere the flow was strongly from the west, while the SH flow was light and without organization. This is reflected in the vertical homogeneity of the SH air with low O_3 and elevated H_2O throughout the troposphere.

The second major transition between air masses occurred

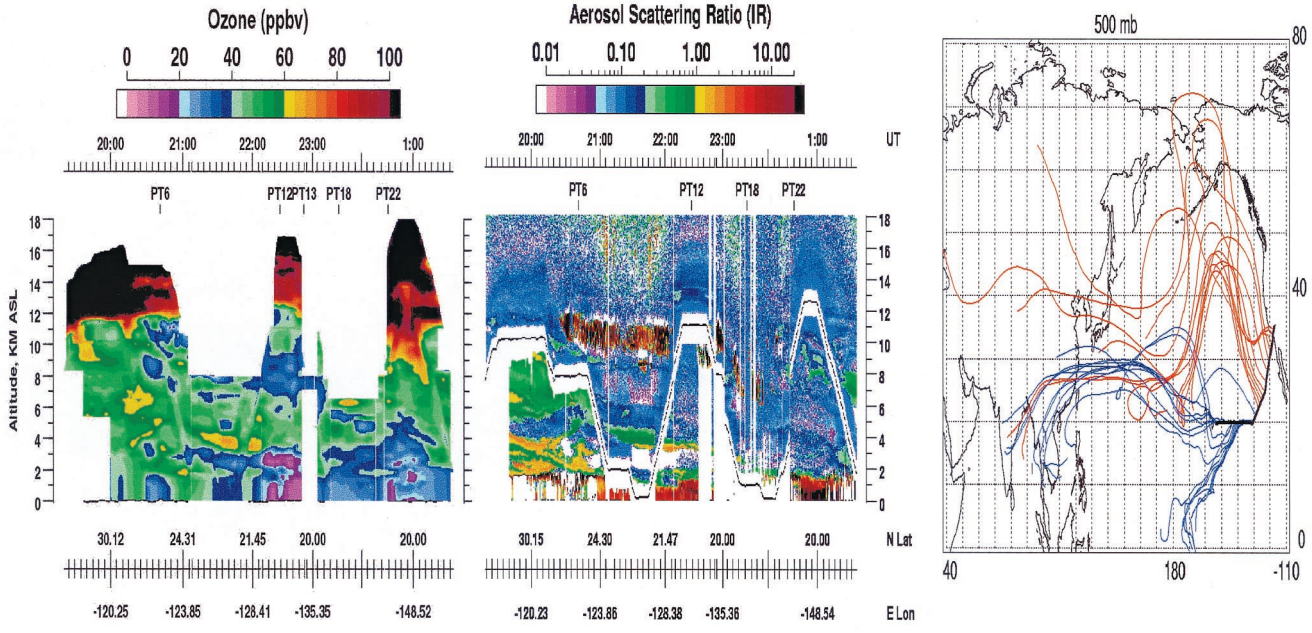

Plate 2. Ozone and aerosol scattering ratio distributions observed on flight from California to Hawaii on March 6–7, 1999 (flight 5). The time (UT), north latitude (N Lat), and east longitude (E Lon) of the measurements are shown. Ten-day back trajectories arriving along the flight track at 500 mbar are also shown with a change in color at 22°N to accentuate the different back trajectory patterns.

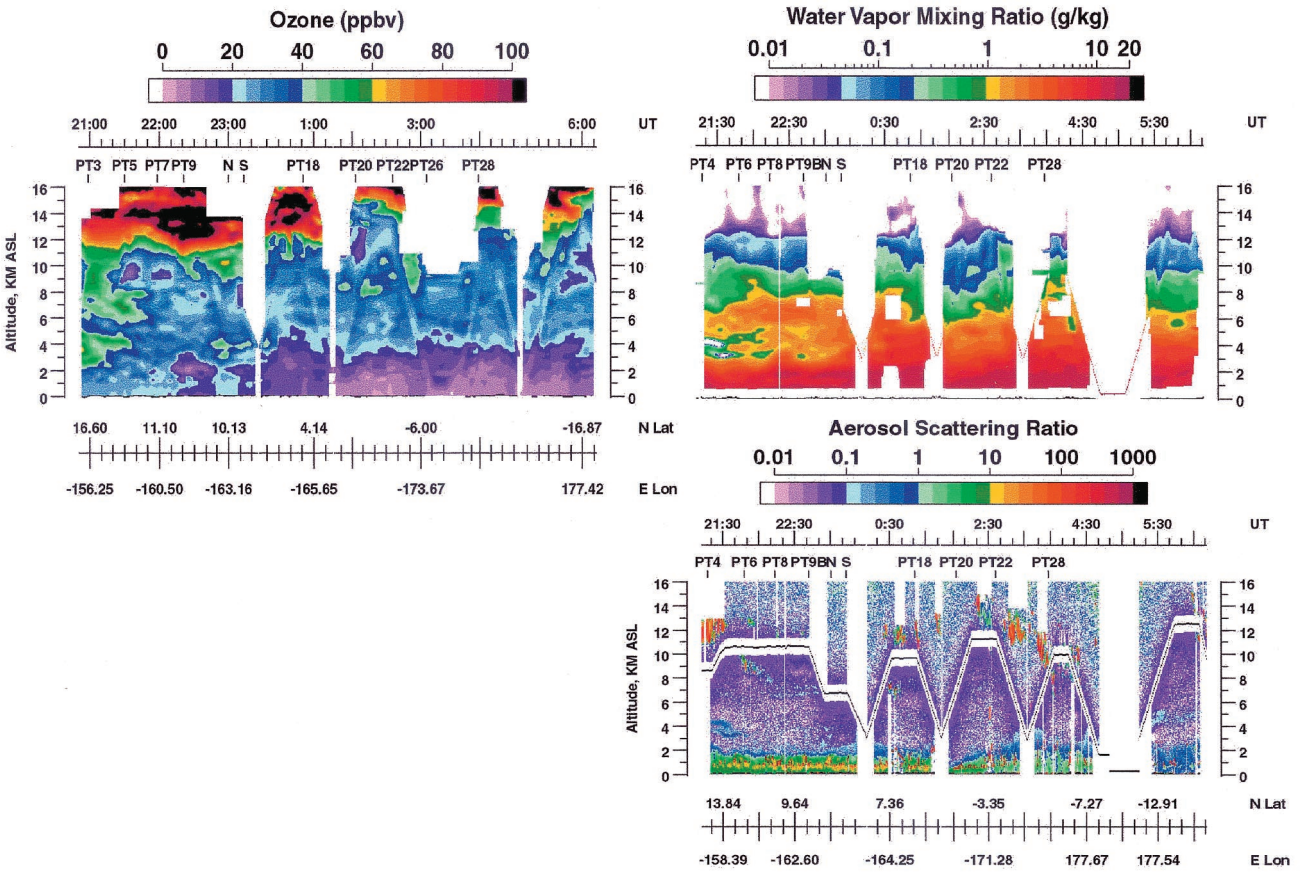

Plate 3. Ozone, H_2O, and aerosol scattering ratio distributions observed across the ITCZ on flight from Hawaii to Fiji on March 17–18, 1999 (flight 9).

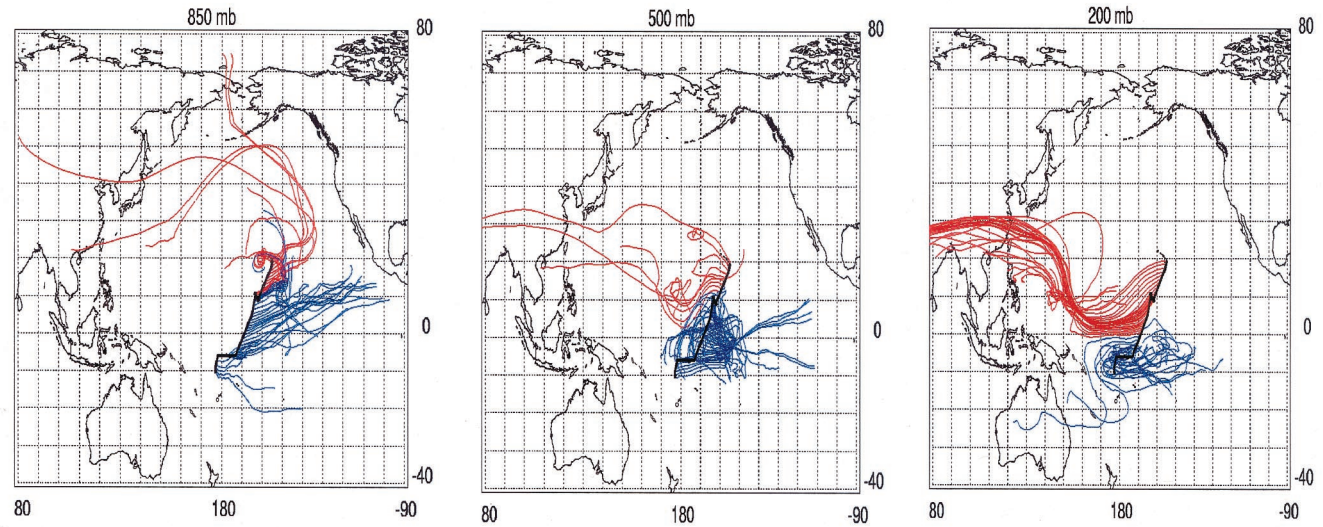

Plate 4. Ten-day back trajectories arriving at 200, 500, and 850 mbar along the flight track corresponding to measurements shown in Plate 3. Different colors are used to accentuate the differences in the back trajectories on either side of the ITCZ at about 10°N.

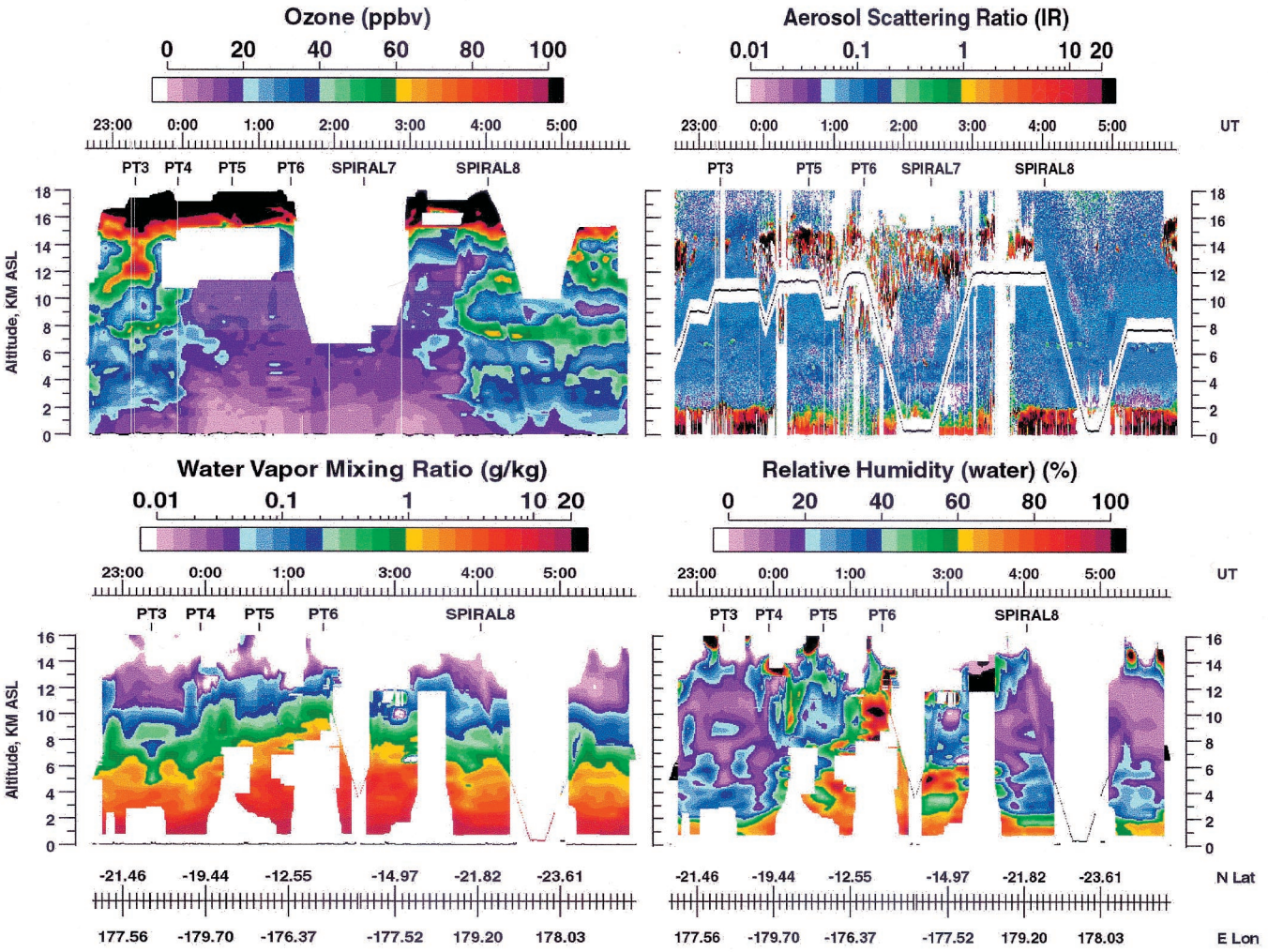

Plate 5. Ozone, aerosols, H_2O, and relative humidity distributions observed across SPCZ on local flight from Fiji on March 20, 1999 (flight 10).

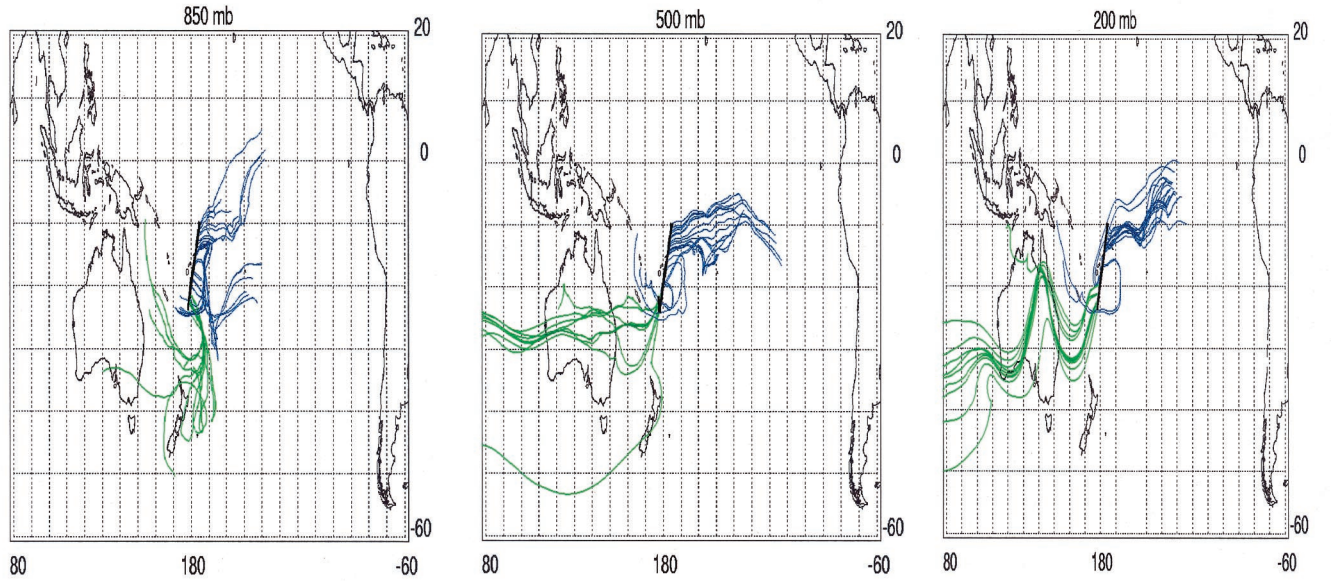

Plate 6. Ten-day back trajectories arriving at 200, 500, and 850 mbar along the flight track corresponding to measurements shown in Plate 5. Different colors are used to accentuate the differences in the back trajectories on either side of the SPCZ.

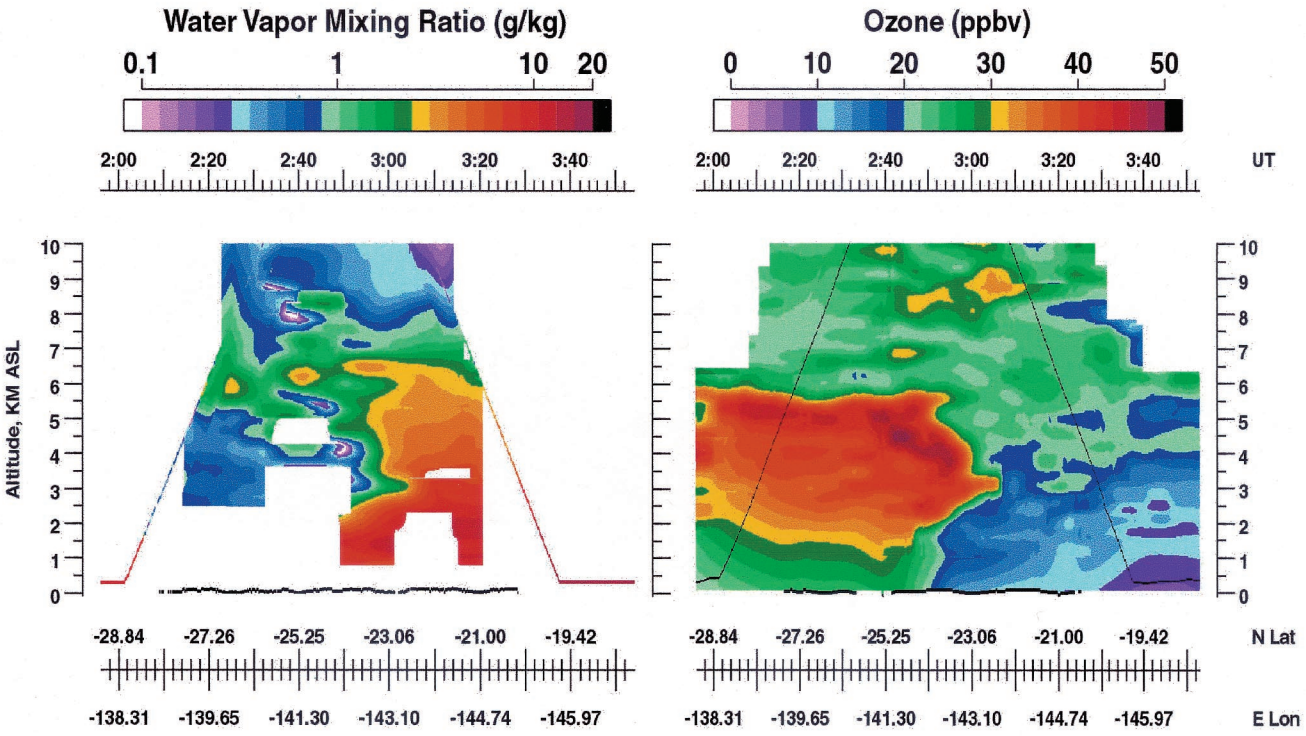

Plate 7. Water vapor and O_3 distribution across SPCZ on local flight from Tahiti on March 31, 1999 (flight 14).

across the South Pacific Convergence Zone (SPCZ) [*Fuelberg et al.*, this issue]. Cross sections from the Fiji local flight on March 20, 1999 (flight 10), show the differences across this region (Plate 5). The flight began south of the SPCZ and crossed the SPCZ twice (at about 0000 and 0350 UT). Ozone decreased by over a factor of 2 from south to north of the SPCZ, and H_2O was again anticorrelated with O_3. Thin cirrus clouds were ubiquitous north of the SPCZ, and there is indication of a change in boundary layer aerosol scattering characteristics in this region. Relative humidity (RH) was calculated from the LASE H_2O and MTP temperature measurements, and the relative change in RH across the SPCZ is much greater than for the H_2O mixing ratio. The large RH values throughout the troposphere correlate with the low O_3 across the region, and modeling studies [*Crawford et al.*, this issue] have shown that O_3 loss is expected to dominate at all altitudes under these conditions. The back trajectory analysis for this case is shown in Plate 6. North of about 20°S, air parcels generally come from the east at all altitudes with long residence times over the Pacific. South of 20°S the air originates mainly from the west with light winds at the surface and stronger westerly winds at higher altitudes. This change in air masses across the SPCZ produces a marked difference in the chemistry and meteorological parameters with the air south of the SPCZ having more of a continental influence than the tropical Pacific air north of the SPCZ. This is very similar to the change in conditions across the ITCZ. An additional example of the transition across the SPCZ was obtained on March 31 during a local flight from Tahiti (flight 14). The H_2O and O_3 distributions observed across the SPCZ are shown in Plate 7. The drier air with enhanced O_3 south of the SPCZ is in contrast with the moister air with lower O_3 to the north of this convergence region. The H_2O increased nearly an order of magnitude near the surface, while O_3 decreased more than a factor of 3 below 6 km. This further indicates the differences that can exist between the chemistry and composition of the two air masses.

Stratospheric intrusions also contribute to determining the composition of the southern midlatitude air. The best example occurred on April 10–11, 1999, on a local flight southwest of Tahiti (flight 18). The O_3, H_2O, RH, and aerosol/cloud observations from that flight are presented in Plate 8. Also shown on each plot are isopleths of potential vorticity (PV) interpolated along the flight track from European Centre for Medium-Range Weather Forecasts (ECMWF) analyses which are done on a 6-hour basis at 31 levels on a 1° by 1° grid. The PV analyses agree well with the general O_3 features observed in the intrusion even though the PV analyses do not have the spatial resolution of the lidar data. On the basis of the PV analyses, enhancements of 8–16 ppbv in O_3 from the stratosphere would be expected down to near the surface assuming a relative factor in the lower stratosphere of about 4.2 ppbv PVU^{-1}, where $PVU = 10^{-7}$ K m^2 kg^{-1} s^{-1} [*Fenn et al.*, 1999] (discussion in section 3.3). There is some indication that the O_3 distribution in the lower troposphere is enhanced by the intrusion. This is not to ascribe all of the variation to this or another upwind intrusion; however, there is reason to attribute some of the O_3 enhancement to a stratospheric source. We will address this later in this paper. Cirrus clouds are located on the equatorward side of the intrusion with cloud tops reaching the local tropopause altitude. The H_2O distribution shows a moister troposphere on the north side of the intrusion and a generally drier atmosphere near the intrusion. The RH distribution shows the location of the intrusion better than the H_2O distribution. The low RH values (<10%) associated with the intrusion are much smaller than the moderate (>40%) to high

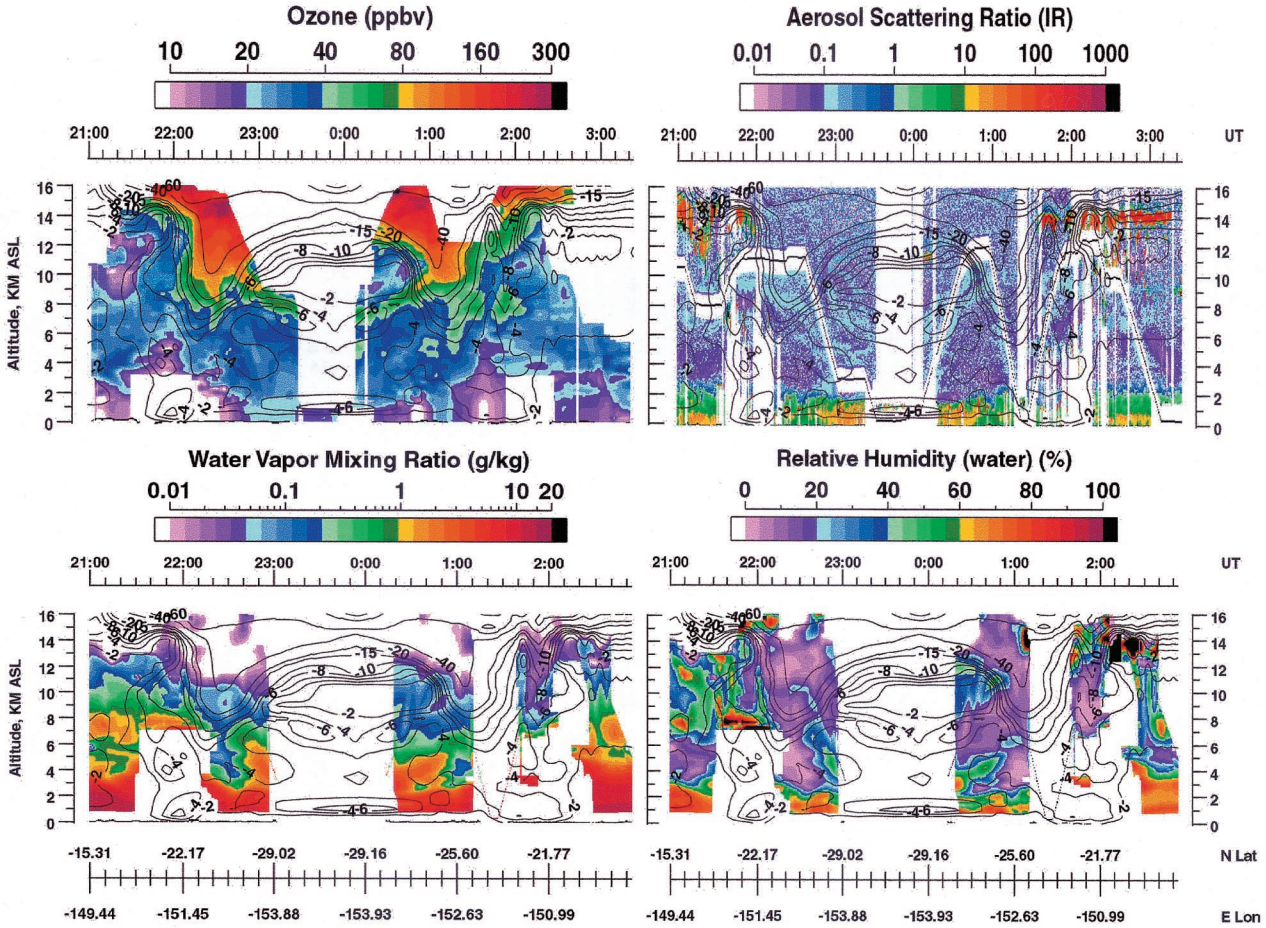

Plate 8. Ozone, aerosols, H_2O, and relative humidity observed across a front and in the vicinity of a stratospheric intrusion on local flight from Tahiti on April 10–11, 1999 (flight 18). Isopleths of potential vorticity (PV) in units of 10^{-7} K m^2 kg^{-1} s^{-1} are overplotted on each distribution for comparison.

(>70%) values seen outside the intrusion with large RH values even near the tropopause in vicinity of the cirrus clouds.

The final flight of PEM-Tropic B from Costa Rica to California revealed air mass characteristics ranging from clean tropical marine air to continental air with a combination of aerosol and pollution sources. Plate 9 shows the O_3, aerosol, H_2O, and RH distributions for flight 22 on April 18, 1999. South of about 13°N the distributions of these parameters show a tropical marine environment that is very moist, with low O_3 in the boundary layer and lower troposphere, and low aerosol loading in the free troposphere. There is a transition in atmospheric conditions in the mid and lower troposphere between 13°N and 22°N. Ozone generally increases along this leg north of 13°N, and the aerosol loading also increases up to a depth of 10 km near 34°N. The H_2O gradually decreases across this region, and the RH shows the greatest change from near-saturation conditions in the tropical marine air to very dry conditions (<10%) in the air having considerable aerosol loading. Cirrus clouds were observed during the middle of this flight with bases as low as 10 km and tops as high as 15 km. Plate 10 shows a vertically expanded view of the aerosol scattering ratio, aerosol depolarization, and RH distributions on the northern end of this flight. Aerosol depolarization at 576 nm is derived from the simultaneous detection of the parallel and perpendicular lidar returns backscattered from the atmosphere. The total atmospheric depolarization ratio is the ratio of the perpendicular to parallel lidar returns, and it includes both the depolarization from aerosols and molecules (~1.5% from molecules alone). The aerosol depolarization contribution to the total atmospheric depolarization is then estimated using the total depolarization and the aerosol scattering ratio at this wavelength. The air with the heavy aerosol loading and the very low RH values, starting near the surface near 22°N and extending up to about 4 km near 30°N, exhibits aerosol depolarization values greater than 25% with some exceeding 40%. The power law wavelength dependence of lidar backscattering [*Browell et al.*, 1985] between 576 and 1064 nm was found to be very low (<0.5). These two factors indicate that the aerosols in this region are probably large desert aerosols in agreement with the desert aerosol lidar measurements of *Sasano and Browell* [1989]. Because of their size and concentration, these desert aerosols were thought to originate over a continental source a few days upwind of the flight track.

Ten-day back trajectories at three levels are shown in Plate 11. The trajectories arriving at 850 mbar show that air at the southern end of the flight leg came across Central America from the tropical Atlantic Ocean while the air in the transition region came from the Caribbean. North of about 24°N the air traveled south along a long fetch of desert in the southwestern United States and northwestern Mexico. At 500 mbar the

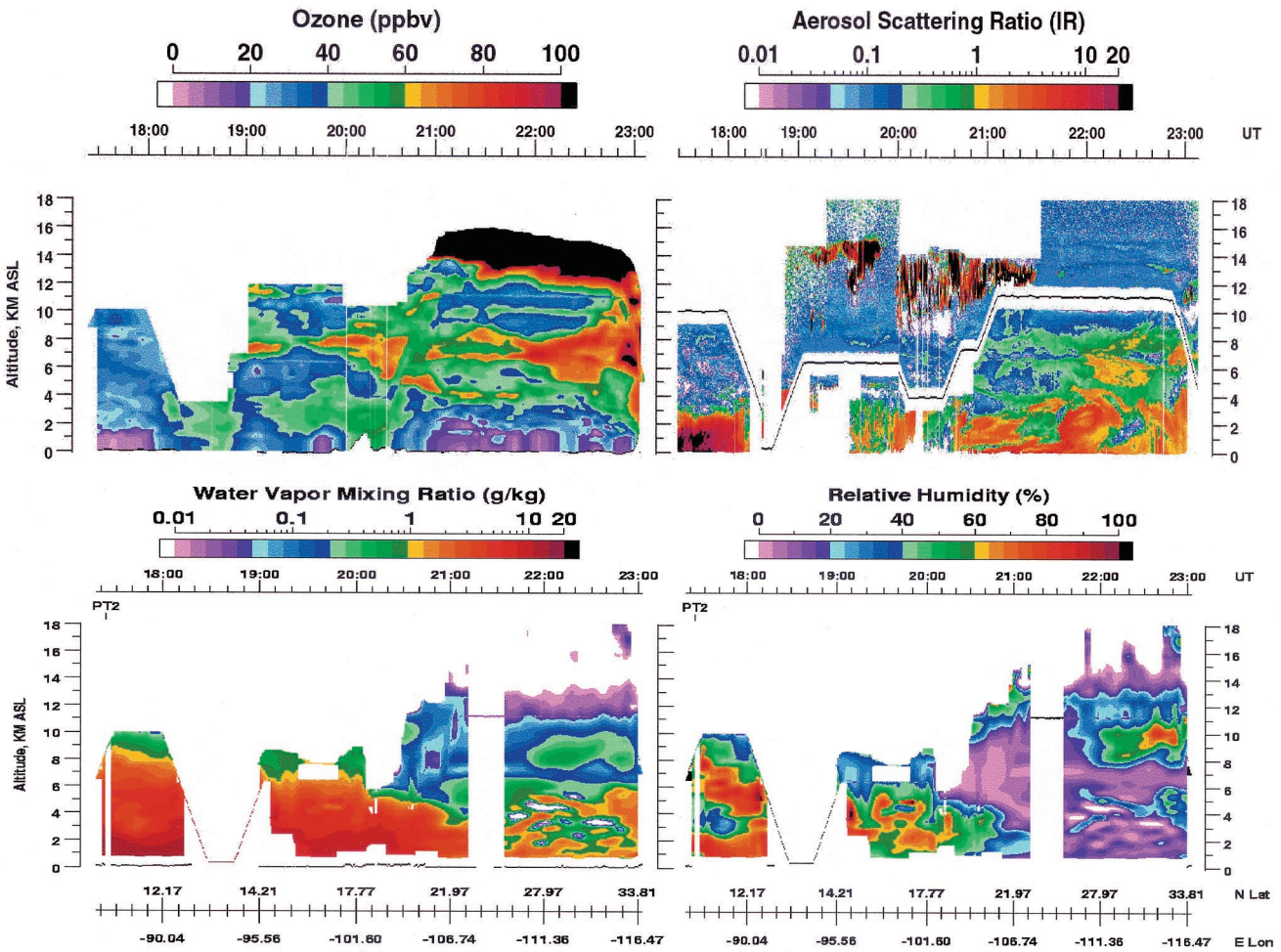

Plate 9. Ozone, aerosol scattering ratios, H_2O, and relative humidity observed across different air masses on survey flight from Costa Rica to California on April 18, 1999 (flight 22).

source of the air generally was similar to that at lower altitudes. However, at 17°N the flow changed direction with the air then coming from the tropical Pacific. North of 28.5°N the flow was from the west with a source from somewhere over Asia or possibly Europe [*Newell and Evans*, 2000]. The upper altitude flow was similar to that at 500 mbar, but the flow on the southern end of the leg was now more from the tropical Pacific. Flight 22 is an excellent example of how major variations in air mass source regions contribute to the composition and chemistry of the atmosphere along a cross section of the atmosphere.

3.2. Average Ozone and Water Vapor Distributions and Correlations

Average latitudinal and longitudinal O_3 cross sections were produced from average O_3 cross sections obtained from each flight. The O_3 profiles from each entire flight, including the interpolated and extrapolated O_3 levels, were averaged in each 0.25°-latitude or 0.50°-longitude bin to produce a single average O_3 profile per bin. The individual flights were then averaged together with equal weighting to get a mission average O_3 profile for each bin [*Browell et al.*, 1996b]. Plate 12 shows the average latitudinal and longitudinal O_3 cross sections obtained for PTA and PTB. The ranges of the averages were chosen to obtain a latitudinal cross section representing the central Pacific (170°W to 120°W) and a longitudinal cross section representing the southern tropical Pacific (30°S to 0°N).

Differences in the large-scale O_3 distribution between PTA and PTB are clearly evident in Plate 12. The extensive burning in Africa, South America, and many other regions during the austral winter (see, e.g., *Olson et al.* [1999] for PTA) contributes to the increased photochemical O_3 production that was observed downwind over the remote central Pacific during PTA [*Fenn et al.*, 1999; *Fuelberg et al.*, 1999; *Schultz et al.*, 1999; *Talbot et al.*, 1999; *Singh et al.*, 2000]. Compared to PTB, the SPCZ in PTA was closer to the ITCZ and did not extend as far southeast. Differences also were found in mid to upper tropospheric flow patterns [*Fuelberg et al.*, 1999, this issue] which allowed for more of a westerly flow of SH biomass burning products and enhanced O_3 across the Pacific during PTA. The enhanced O_3 from biomass burning can be seen throughout the troposphere south of 10°S, and this extends north to nearly the ITCZ at about 9°N. Enhanced O_3 levels in the NH air to the north of the ITCZ can be seen in the plate. The region of very low O_3 (<20 ppbv) was from 6°S to 18°N near the surface, and low O_3 was also found in the upper troposphere due to convection principally occurring near the ITCZ. The longitudinal O_3 distribution during PTA shows the general transport of the biomass burning plumes to low latitudes in the central

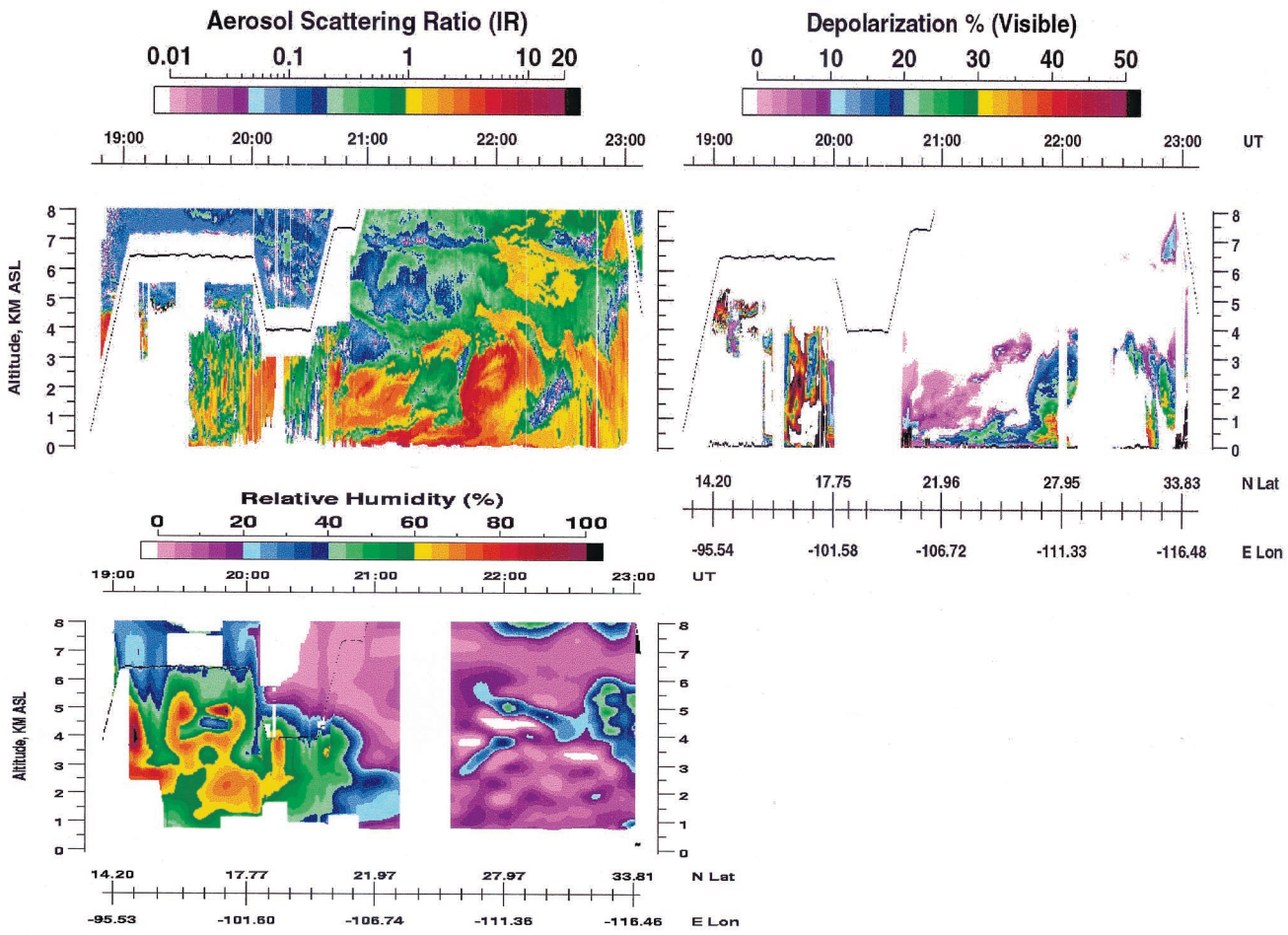

Plate 10. Aerosol scattering ratio, aerosol depolarization, and relative humidity for the same flight shown in Plate 9.

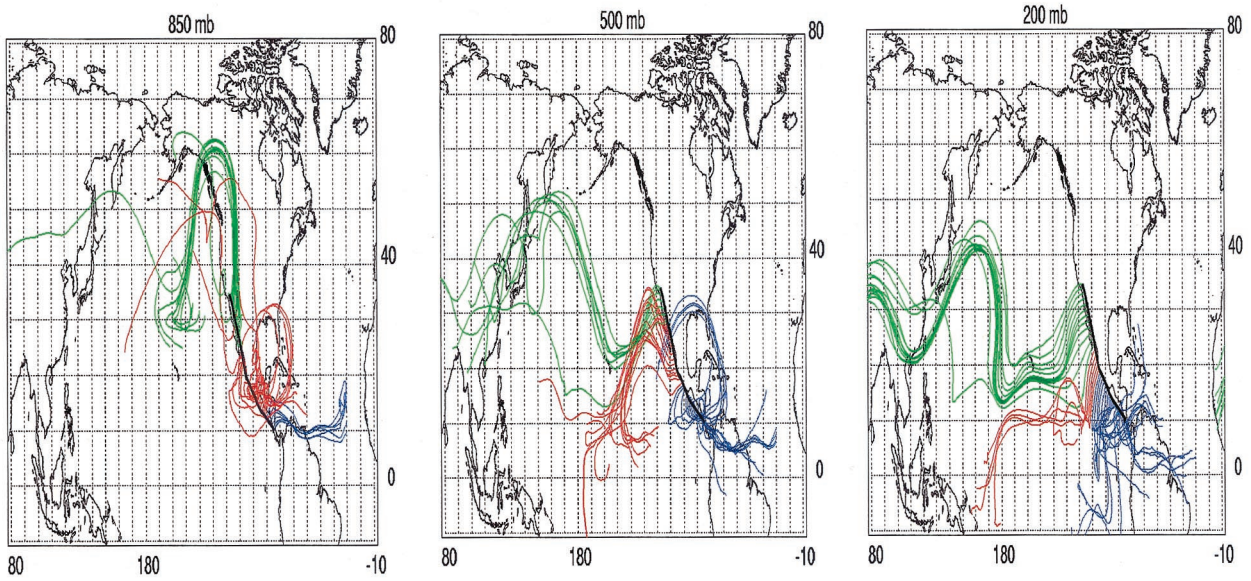

Plate 11. Ten-day back trajectories arriving at 850 mbar along the flight track from Costa Rica to California on April 18, 1999 (see measurements shown in Plates 9 and 10). Different colors are used to show the back trajectories for three regions having distinctly different air mass histories along the flight track.

Pacific with the region of very low O_3 being most extensive in the western Pacific. Transport of biomass burning plumes across the Pacific in the westerlies is also indicated in the enhanced O_3 distribution in the midtroposphere in the eastern Pacific.

The latitudinal O_3 distribution from PTB (Plate 12) clearly shows the average location of the ITCZ and SPCZ across the central Pacific. The enhanced O_3 throughout the troposphere in the NH air north of the ITCZ at about 12°N contrasts with the low O_3 throughout the troposphere in the SH air from there to the SPCZ at about 22°S. The air south of the SPCZ exhibited enhanced O_3 from stratospheric intrusions and continental sources, although in contrast to PTA, there was very little biomass burning in the SH during PTB [*Blake et al*., this issue]. The longitudinal distribution shows the largest region of very low O_3 in the western Pacific, but unlike PTA, the very low O_3 region extended across the entire Pacific at low altitudes. Ozone was low (<30 ppbv) across the entire region from the surface to the tropopause which decreased in altitude to the east from 15 to 12 km.

Average latitudinal and longitudinal H_2O distributions were constructed from the remote LASE measurements employing the same techniques used for the O_3 distributions. The H_2O distributions for PTB are shown in Plate 13. The change in H_2O across the ITCZ near 12°N can be seen in the decrease in altitude of the 1 g kg^{-1} level from about 7 to 4 km. Water vapor levels in the marine boundary layer were significantly lower north of the ITCZ. The SPCZ is much more difficult to see in the average H_2O distribution, but the transition occurs in the region from 18° to 24°S. The change in H_2O to the east across the Pacific shows a general drying of the troposphere at all altitudes with the largest changes being below 4 km.

Composite average H_2O and O_3 profiles for PTB were calculated for the NH air north of 15°N, the SH tropical Pacific air between 10°N and 20°S, and the SH subtropical air south of 25°S with the results presented in Plate 14. The H_2O is considerably higher in the SH tropical Pacific, particularly in the mid to upper troposphere. There is no statistically significant difference in our observed H_2O profiles for the NH air and SH subtropical air above 2 km. Near the surface the SH subtropical air appears to be slightly drier than the NH air. The O_3 profile for the SH tropical Pacific was lower than the other two regions at all altitudes. This profile starts at 12 ppbv near 1 km and does not exceed 28 ppbv until above 11 km. The SH subtropical O_3 profile is less than 10 ppbv greater than the SH tropical Pacific O_3 profile up to about 8 km where the lower tropopause and stratospheric intrusions make a significant contribution at higher southerly latitudes. The NH O_3 profile shows a more significant O_3 enhancement throughout the mid to lower troposphere than either of the other profiles, and this difference was maintained compared to the SH tropical Pacific profile to above 11 km.

Correlations between H_2O and O_3 were examined to better quantify differences in the three regions, and these results are shown in Plate 15. There was no statistical difference between the correlations at H_2O levels greater than 1 g kg^{-1} which is predominantly air below 5 km in the SH subtropics and below 7.5 km in the SH tropical Pacific. The correlation changed in the upper troposphere of the SH subtropics (>5 km) as this air had more stratospheric influences. The H_2O to O_3 correlation was distinctly different for the NH air which was driven by the very different air mass origins. This was true for H_2O greater than 0.1 g kg^{-1} compared to SH tropical Pacific and greater than 1 g kg^{-1} compared to SH subtropics. These results suggest a clear delineation between the SH and NH air masses with respect to H_2O and O_3, but the distinction between the SH subtropical air south of the SPCZ and the SH tropical Pacific air is more difficult to make on average possibly due to the limited sampling of air in the former category or the variability in the location or strength in the SPCZ.

3.3. Air Mass Characterization

3.3.1. Air mass types and observations. A general categorization of air masses observed during PTB was done by using a variation of the principal component analysis on the O_3 and aerosol distributions measured with the UV DIAL system and the PV values along the flight track derived from meteorological analyses from ECMWF data (details of this approach have been previously discussed by *Browell et al*. [1992, 1996a, 1996b] and *Fenn et al*. [1999]). Since the background or reference air in the SH tropical Pacific during PTB was much different from that during PTA [*Fenn et al*., 1999], a different reference O_3 profile was chosen as a discriminator. The reference O_3 profile was selected to approximate the average in situ O_3 profile between 10°S and 10°N. This average in situ O_3 profile and the selected O_3 discriminator are shown in Figure 2. The average in situ profiles for these regions are very similar to those shown in Plate 14 for the more extensive measurements combining the remote and in situ O_3 measurements. These profiles also compared well to the average O_3 profiles obtained from ozonesondes launched from Tahiti, Fiji, and Samoa during this field experiment [*Oltmans et al*., this issue; *Raper et al*., this issue]. Thus, for the purposes of air mass identification, the O_3 discriminator was assumed to represent the background or reference O_3 profile over the tropical Pacific during the experiment. The various air mass types are then judged against this reference O_3 profile with additional differentiation using aerosol backscatter and PV. Nine categories of air masses were identified using this technique. These current air mass categories are similar to those in our PTA analysis [*Fenn et al*., 1999]. The air mass types and their criteria are as follows: reference (REF), ozone levels within 20% of the reference profile and low IR aerosol scattering ratios ($S < 0.2$); background plume (BPLU), same as REF except with enhanced aerosols ($S > 0.2$); near surface (NS), air with high aerosol loading associated with boundary layer; clean Pacific (CP), ozone more than 20% below the reference profile and $S < 0.2$; convective outflow (CON), same as CP except cirrus clouds are in the vicinity; high-ozone plume (HPLU), ozone more than 20% above the reference profile and $S > 0.2$; high ozone (HO3), ozone more than 20% above the reference profile, $S < 0.2$, and amount of O_3 attributable to stratosphere is <25%; high-ozone mixture (HO3M), same as HO3 except the amount of O_3 attributable to stratosphere is 25–60%; stratospherically influenced (SINF), same as HO3 except that the amount of O_3 attributable to stratosphere is >60%. Note that in the calculation of the amount of O_3 attributed to the stratospheric component it is assumed that the O_3 in the lower stratosphere has the following approximate relationship to PV: O_3 [ppbv] ~4.2 ppbv × |PVU| [*Fenn et al*., 1999] (discussion at end of section).

UV DIAL O_3 and aerosol measurements and ECMWF-derived PV values were used to categorize the air masses for each flight by geographic location and altitude. An example of the air mass characterization done for the first half of flight 18 on April 10–11, 1999, is presented in Plate 16. Ozone, aerosols,

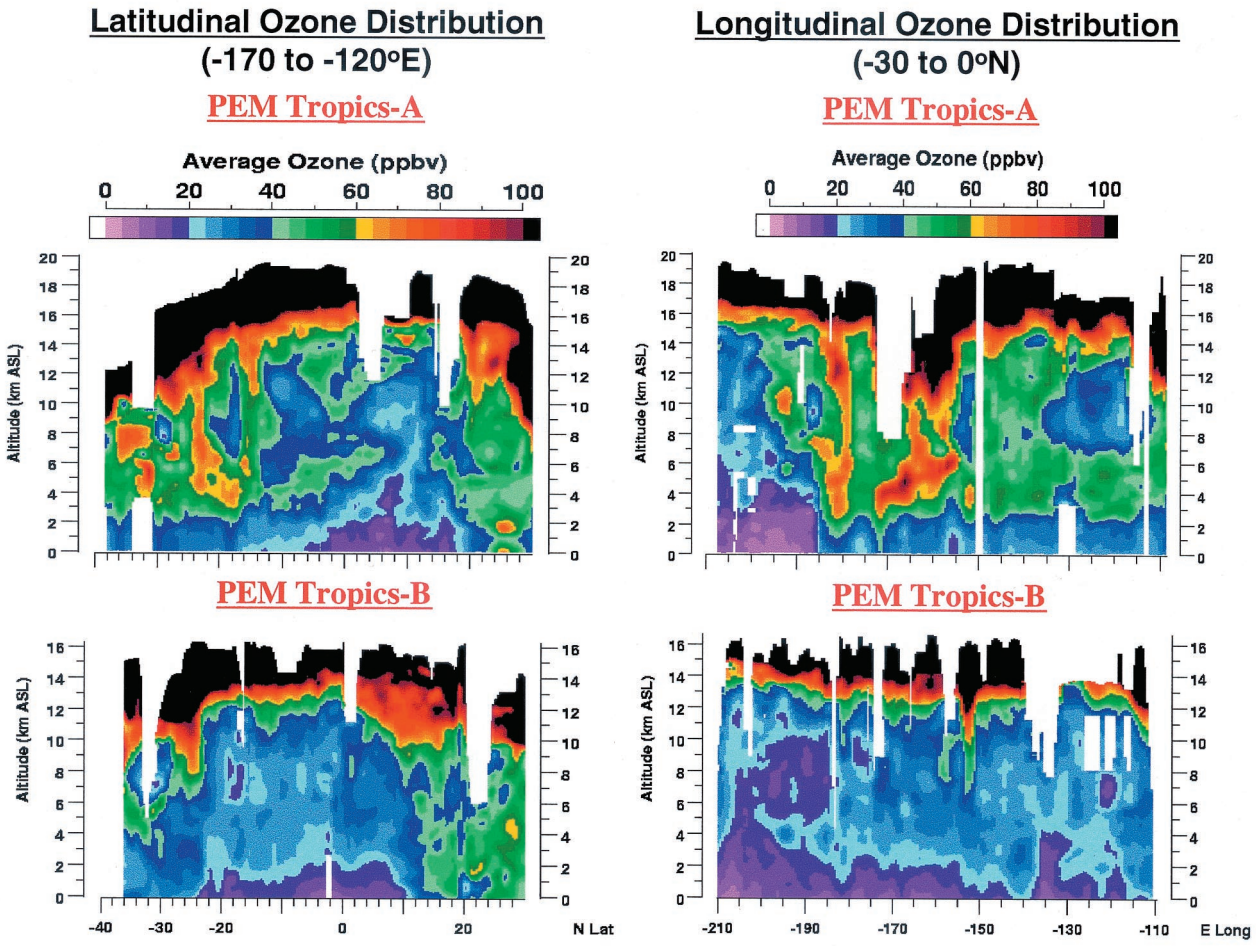

Plate 12. Comparison of average latitudinal and longitudinal O_3 cross sections observed during PEM-Tropics A and B.

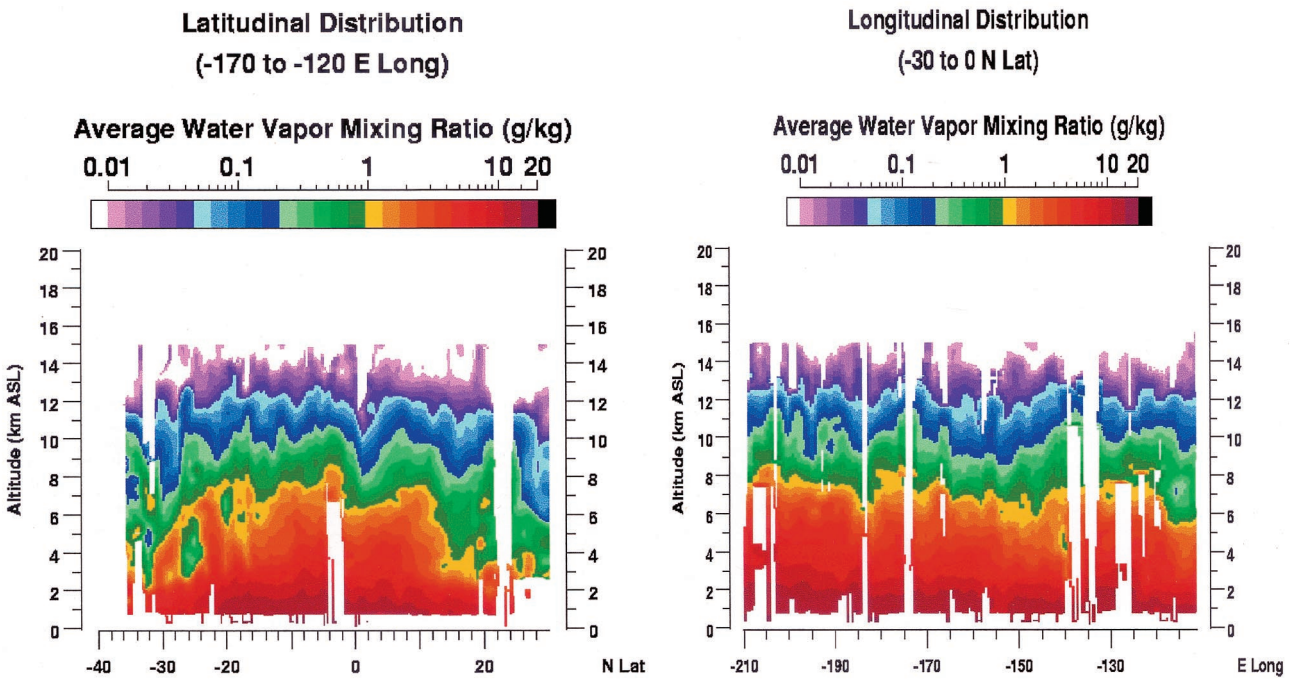

Plate 13. Average latitudinal and longitudinal H_2O distribution observed during PEM-Tropics B.

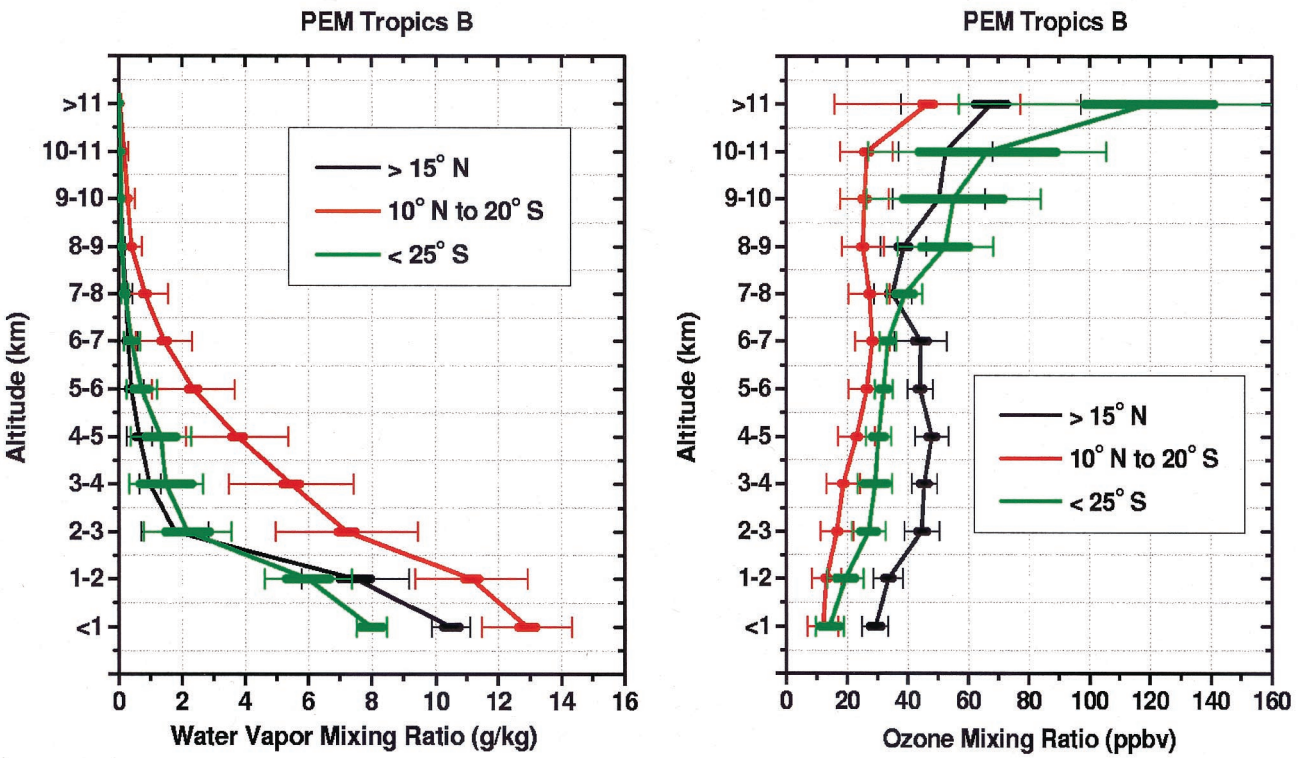

Plate 14. Average H_2O and O_3 profiles observed during PEM-Tropics B (flights 6–18) in NH air north of 15°N, in SH tropical air from 10°N to 20°S, and in SH subtropical air south of 25°S. Thick and thin whiskers indicate $\pm 2\sigma_{ave}$ (σ_{ave} = standard error of the average) and $\pm 1\sigma_{std}$ (σ_{std} = standard deviation of the measurements), respectively.

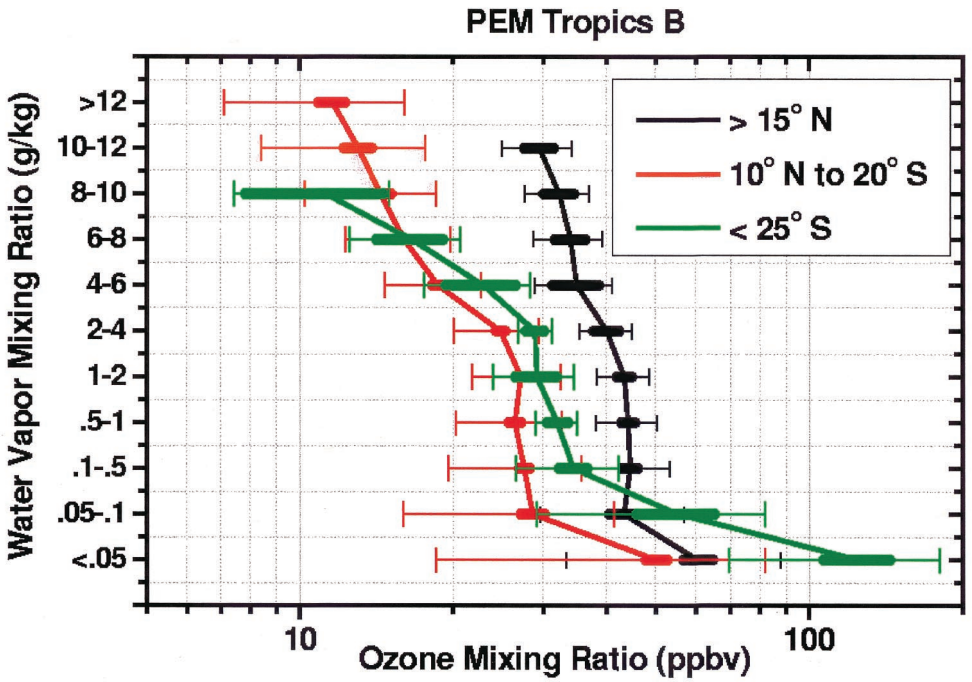

Plate 15. Average H_2O/O_3 correlations in the different domains defined in Plate 14. Thick and thin whiskers indicate $\pm 2\sigma_{ave}$ (σ_{ave} = standard error of the average) and $\pm 1\sigma_{std}$ (σ_{std} = standard deviation of the measurements), respectively.

Table 1. Average NH Air Mass Composition (Mean/Median (Number of Cases))[a]

	Air Mass Type				
Parameter	REF (8)	NS (8)	HO3 (13)	HO3M (9)	SINF (1)
Altitude, km	6.49/7.08	0.72/0.62	7.22/7.61	7.76/7.67	10.97
RHW, %	40.8/39.4	72.1/71.7	25.9/24.3	22.5/17.4	11.1
RHI, %	37.6/35.7	70.4/68.2	23.4/20.5	19.8/14.3	9.5
O_3, ppbv	22.8/23.3	17.4/11.9	39.4/40.1	41.5/41.4	83.8
CO, ppbv	66.7/64.6 (7)	84.6/81.5	73.7/76.8	77.7/72.6	76.2
CH_4, ppbv	1729.8/1737.2 (6)	1760.8/1757.8	1746.4/1751.8 (9)	1750.3/1752.7 (7)	1744.4
CO_2, ppmv	367.85/367.91	368.84/368.80	367.91/368.08	368.00/368.01	366.80
C_2H_2 (ethyne)	43.5/36.2 (7)	56.3/46.5 (7)	73.2/72.8	53.2/56.3 (6)	97.4
C_2H_4 (ethylene)	7.80 (1)	15.19/11.62 (5)	4.28/3.60 (5)	···	···
C_2H_6 (ethane)	458/406 (5)	717/663	570/565	565/516 (8)	···
C_3H_8 (propane)	30.0/15.5 (7)	106.5/48.2	43.4/34.8	39.9/30.0 (8)	47.8
PAN	35.6/24.9 (7)	10.0/4.8 (5)	63.3/54.4	90.4/70.1 (8)	90.3
SO_2	52.9/45.5 (4)	275.1/46.5 (6)	79.1/28.2 (9)	31.6/26.0 (6)	34.7
DMS	4.2/4.6 (3)	28.1/9.2	1.2 (1)	···	···
NO	11.6/14.8 (7)	···	16.0/17.1 (12)	12.8/8.8 (8)	11.3
NO_2	4.4/4.4 (5)	3.9/2.2 (3)	8.1/8.4 (8)	12.1/5.2 (3)	···
HNO_3	48.5/53.3 (5)	98.0/41.4	85.3/74.9	63.4/68.2 (8)	···
OH, 10^6 cm^{-3}	0.210/0.222	0.250/0.057 (5)	0.197/0.185	0.143/0.195	0.209
HO_2	12.32/11.30	9.81/10.86	5.69/9.51	8.17/11.41	4.59
H_2O_2	569/433	990/776	361/327	380/363	143
HCHO	151/111 (7)	337/337	141/124 (10)	348/118 (7)	97.3
CH_3Cl	562.2/558.0 (7)	574.3/568.6	570.5/573.0	570.2/568.4 (7)	573.6
CH_3Br	8.72/8.80 (7)	9.26/9.43	9.05/9.11	9.28/9.22 (8)	9.00
CH_3CCl_3	60.83/61.04 (7)	61.8/61.6	61.5/61.8	66.4/61.8 (8)	61.8
CH_3I	0.120/0.136 (7)	0.401/0.425	0.107/0.086	0.091/0.097 (8)	0.091
$CHBr_3$	0.615/0.655 (7)	1.229/0.961	0.488/0.465	0.373/0.417 (8)	0.220
C_2Cl_4	2.10/2.10 (7)	2.13/2.23	1.77/2.03	1.62/1.55 (8)	1.28
UFA, cm^{-3}	3249/2688	465/372	2736/2780	2382/2541	3144
FAU, cm^{-3}	2022/1788	432/348	1905/1837	1874/1986	1778
Nitrate	···	67.6/54.0 (7)	12.0 (1)	···	···
Sulfate	108.7/22.6 (5)	190.1/100.5	25.1/25.0 (9)	24.2/23.0 (5)	38.0
^7Be, fCi/scm	413/322 (3)	198/142 (7)	478/424 (9)	500/415 (5)	1346
FAU/UFA	0.73/0.80	0.92/0.97	0.85/0.83	0.83/0.84	0.57
C_2H_2/CO[b]	0.60/0.59	1.16/0.90	0.93/0.95	1.00/0.82 (8)	1.28
C_3H_8/C_2H_6	0.055/0.043 (8)	0.096/0.068	0.066/0.050	0.063/0.057 (8)	···
O_3/CO	0.36/0.34	0.29/0.11	0.55/0.54	0.53/0.50	1.10
SO_4/O_3[b]	5.04/1.47 (7)	17.9/9.2	0.66/0.64 (9)	0.60/0.63 (5)	0.45
NO_2/O_3[b]	0.19/0.19 (6)	0.46 (2)	0.22/0.20 (8)	0.20/0.16 (5)	···
$^7Be/O_3$[c]	14.0/13.4 (6)	17.6/14.3 (7)	12.9/11.1 (8)	11.8/10.9 (5)	16.1

[a]Values are in pptv unless otherwise noted; UFA, ultrafine aerosols; FAU, unheated fine aerosols.
[b]Units of pptv/ppbv.
[c]Units of (fCi/scm)/ppbv.

H_2O, and RH were presented for this flight in Plate 8. The air mass classification method identified a large portion of the air above 2 km as having a strong stratospheric influence (SINF). There are enhanced O_3 regions where the stratospheric component explains a moderate amount of the enhanced O_3 (HO3M), and a few small regions where there was very little stratospheric contribution (HO3). It is clear that the relatively low-resolution PV analyses cannot map all the features that the DIAL system observes. Thus there is some unavoidable misrepresentation of air masses between these groups in the vicinity of highly structured intrusions. This example also indicates air associated with deep convection with its associated low O_3 and cirrus clouds (CON), near-surface air up to about 3 km (NS), and reference air (REF) predominantly on the equatorward side of the intrusion.

The results from each flight were grouped together based on the regions identified in Figure 1. The 5°N latitude line separating the NH regions from the SH low-latitude regions was chosen because it represented an approximate average location of the northern branch of the ITCZ. Also, several of the regions are the same as those used previously in the PTA air mass analysis [*Fenn et al.*, 1999] to permit comparisons between the field experiments. Plate 17 presents results for all of the PTB regions. The contrast in the air mass types identified in the NH (CPNH and EPNH) compared to the low-latitude cases (CPLL and EPLL) is readily apparent. There is a significant amount of enhanced O_3 that is not attributed to stratospheric influence (HO3) in the NH. In the EPNH the amount of enhanced O_3 associated with enhanced aerosols increases significantly over the CPNH. There is some contribution from the stratosphere in the mid to low troposphere over the CPNH. At low latitudes over the central Pacific (CPLL) and eastern Pacific (EPLL), the situation is similar with the background or reference air dominating the distribution below 10 km. Additional contributions (up to ~20%) come from low O_3 air associated with convective outflow (CON), enhanced O_3 air resulting from photochemical production (HO3), and enhanced O_3 air resulting from a mixture of photochemical O_3 production and some stratospheric influence (HO3M). In the western Pacific low latitudes (WPLL), convective outflow of low O_3 (CON) into the 3 to 13 km region is a major factor in determining the distribution of O_3 in the mid to upper troposphere.

Table 2. Average SH Air Mass Composition (Mean/Median (Number of Cases))[a]

Parameter	Air Mass Type					
	REF (34)	NS (13)	HO3 (2)	HO3M (4)	SINF (2)	CON (12)
Altitude, km	7.23/7.12	0.63/0.60	6.71	4.98/4.28	10.23	8.31/8.80
RHW, %	42.7/42.7	77.3/77.5	19.4	29.1/28.6	32.5	49.7/52.4
RHI, %	37.4/36.0	75.4/76.2	16.3	26.1/25.6	31.2	42.5/46.0
O_3, ppbv	23.5/23.6	11.6/10.8	34.0	24.1/28.2	74.8	15.8/15.9
CO, ppbv	48.8/46.4 (33)	51.6/45.0 (11)	58.8	50.7/49.7	38.1	50.8/48.8 (11)
CH_4, ppbv	1717.9/1714.6 (29)	1720.4/1711.3 (11)	1730.9	1719.9/1717.2	1703.3	1718.4/1717.7
CO_2, ppmv	366.72/366.69	366.38/366.09	366.53	366.62/366.64	365.56	366.74/366.70
C_2H_2 (ethyne)	18.6/15.9 (25)	19.6/13.5 (11)	26.4	21.6/18.5	8.71	19.4/14.4
C_2H_4 (ethylene)	4.52/3.80 (11)	6.07/6.62 (5)	···	···	···	4.26 (2)
C_2H_6 (ethane)	268/241 (25)	264/210 (11)	328 (1)	291/272	···	282/263
C_3H_8 (propane)	8.0/5.7 (25)	9.2/6.9 (10)	20.8	8.6/8.0	7.96	8.3/6.5
PAN	18.2/15.8 (32)	17.0/16.8 (11)	72.8	27.8/26.2	···	16.6/14.7 (11)
SO_2	36.6/39.7	25.5/19.8 (12)	34.7	30.8/30.0	28.4	22.1/23.6
DMS	16.4/4.1 (9)	51.6/19.5 (6)	···	2.0 (1)	···	26.6/10.9 (6)
NO	19.2/15.8 (26)	33.8/10.9 (11)	25.7	12.4/9.6	25.2	10.5/7.5
NO_2	6.4/4.9 (14)	4.6/3.7 (7)	11.8	5.8/3.9 (3)	15.6 (1)	7.1/4.2 (6)
HNO_3	42.0/42.2 (31)	44.8/30.2 (10)	54.1	95.4/93.7	177.4 (1)	58.7/41.6
OH, 10^6 cm^{-3}	0.248/0.244	0.095/0.100	0.307	0.339/0.327	0.258	0.267/0.248
HO_2	9.98/10.00	8.87/7.93	10.77	10.80/10.52	4.03	10.24/10.12
H_2O_2	491/337 (31)	822/881	451	481/337	182	419/246
HCHO	125/112 (29)	472/234 (11)	70 (1)	174/83	120	121/113 (10)
CH_3Cl	540.9/539.9 (25)	545.2/538.3 (11)	558.5	546.2/545.4	530.0	538.4/532.8
CH_3Br	8.20/8.10 (25)	8.23/8.10 (11)	8.43	8.30/8.35	8.00	8.26/8.22
CH_3CCl_3	69.97/60.00 (25)	60.4/60.5 (11)	59.7	60.1/60.2	59.9	60.4/60.4
CH_3I	0.155/0.130 (25)	0.286/0.160 (11)	0.085	0.117/0.107	0.091	0.167/0.157
$CHBr_3$	0.571/0.520 (25)	0.644/0.555 (11)	0.397	0.536/0.556	0.400	0.684/0.590
C_2Cl_4	1.41/1.36 (25)	1.30/1.08 (10)	1.23	1.44/1.39	0.84	1.46/1.23
UFA, cm^{-3}	5058/3354	325/280	2439	3638/896	3337	7740/7504 (11)
FAU, cm^{-3}	3081/2420	321/279	1270	2092/980	2123	3675/3754 (11)
Nitrate	21.2/23.5 (8)	19.8/22.4 (10)	1.2 (1)	20.8/24.0 (3)	···	12.9/12.3 (4)
Sulfate	23.7/23.7 (24)	55.2/34.2 (11)	···	430.5 (2)	34.8	23.3/22.0 (11)
^7Be, fCi/scm	336/276 (18)	630/442 (7)	···	347 (1)	3259	327/167 (9)
FAU/UFA	0.66/0.69 (32)	0.84/0.97	0.81	0.87/0.87	0.85	0.70/0.69 (10)
C_2H_2/CO[b]	0.32/0.33 (27)	0.29/0.27 (10)	0.44 (1)	0.41/0.37	0.72	0.27/0.25 (10)
C_3H_8/C_2H_6	0.141/0.029 (26)	0.079/0.042 (11)	0.033	0.028/0.030	0.044	0.029/0.026 (10)
O_3/CO	0.54/0.47 (33)	1.24/0.35 (11)	0.53 (1)	0.63/0.64	2.33	0.31/0.33 (9)
SO_4/O_3[b]	1.67/0.94 (19)	5.62/2.67 (9)	0.36 (1)	1.76/0.70 (9)	0.44	5.70/1.64 (9)
NO_2/O_3[b]	0.26/0.19 (14)	0.27/0.32 (5)	0.32	0.30 (2)	···	0.41/0.25 (5)
$^7Be/O_3$[c]	10.6/9.8 (17)	71.3/58.8 (9)	···	5.9/4.1 (3)	16.6	13.5/11.6 (9)

[a]Values are in pptv unless otherwise noted; UFA, ultrafine aerosols; FAU, unheated fine aerosols.
[b]Units of pptv/ppbv.
[c]Units of (fCi/scm)/ppbv.

Table 3. NH/SH Ratios of Gases by Air Mass Type (Mean/Median)

Species	Air Mass Type			
	REF	NS	HO3	HO3M
O_3	0.97/0.99	1.50/1.10	1.16/1.18	1.72/1.47
CO	1.37/1.39	1.64/1.81	1.25/1.31	1.54/1.46
CH_4	1.007/1.013	1.024/1.027	1.009/1.012	1.017/1.023
CO_2	1.003/1.003	1.007/1.007	1.004/1.004	1.004/1.004
C_2H_2	2.34/2.28	2.87/3.44	2.77/2.76	2.46/3.04
C_2H_6	1.71/1.69	2.71/3.15	1.74/1.72	1.94/1.90
C_3H_8	3.73/2.72	11.64/6.99	2.09/1.67	4.62/3.74
NO	0.60/0.94	···	0.62/0.67	1.03/0.92
NO_2	0.69/0.90	0.85/0.60	0.69/0.71	2.09/1.33
HNO_3	1.15/1.26	2.19/1.37	1.58/1.38	0.66/0.77
HCHO	1.21/0.99	0.71/1.44	1.17/1.10	2.00/1.42
CH_3Cl	1.04/1.03	1.05/1.06	1.02/1.03	1.04/1.04
CH_3Br	1.06/1.09	1.13/1.16	1.07/1.08	1.12/1.10
$CHBr_3$	1.08/1.26	1.91/1.73	1.24/1.18	0.70/0.78
C_2Cl_4	1.49/1.54	1.64/2.06	1.44/1.65	1.13/1.12

The midlatitude regions of the central Pacific (CPML) and the eastern Pacific (EPML) are very similar with the stratospherically influenced air (SINF) contributing to the O_3 budget all the way down to the surface. While the SINF category was decreasing in frequency with decreasing altitude, the amount of HO3M was increasing significantly, which also indicates some stratospheric influence even though it is has been mixed with tropospheric air.

The results from PTA (not shown) [*Fenn et al*., 1999] indicate a dominant influence of enhanced O_3 air masses (>60%) attributed to photochemical O_3 production (HPLU and HO3) at SH midlatitudes in the western and central Pacific (WPML and CPML). These air masses also had a significant impact (>30%) in the midtroposphere even at low latitudes. Convective outflow of low O_3 air from the surface to 7 to 15 km was frequently observed in the central Pacific low-latitude case during PTA, but during PTB it was not observed as often. This might be due to the smaller contrast in O_3 distribution between the surface and the upper troposphere and an O_3 discriminator that possibly made it more difficult to detect this type of air mass.

The average frequency of observation of all SH air mass types is presented in Plate 18 along with the average O_3 profile for each air mass type. The reference air mass type occurred 44–53% of the time from 3 to 10 km, and the average O_3 profile for it was very close to the discriminator O_3 profile. This provided added support for this air mass type being the principal component in the analysis. The balance of the air mass types in this region were mostly distributed between convective outflow (CON), high O_3 (HO3), and high O_3 mixed (HO3M) with CON more prevalent in the upper altitudes and HO3 and HO3M more frequently observed in the lower free troposphere. As was expected, the near-surface air dominated the air mass types below 3 km, and in the upper troposphere the frequency of observations of stratospherically influenced air (SINF) increased with increasing altitude to the average tropopause level above 16 km where it was observed more than 86% of the time. There were few observations in the categories of aerosol plumes with background levels of O_3 (BPLU) or of air with very low O_3 air in the free troposphere that was not associated with convective outflow (CP). The average O_3 profiles for the various air mass types show that at the lowest altitudes in the free troposphere (~1–3 km) the SINF and HO3M categories have the highest average O_3 levels associated with them, while above about 7 km, the SINF category has the highest observed O_3 levels. The HO3 and HO3M categories have similar O_3 profiles above 6 km, while below 6 km, HO3 is comparable to HPLU and NS at even lower altitudes. The CON O_3 profile was constant at about 17 ppbv from about 5 to 13 km, and CP O_3 profile was similar to CON with it decreasing to 5 ppbv at 1 km.

Average PV profiles for each air mass type are also shown in Plate 18. As expected, the SINF category had the highest average PV at all altitudes, and the HO3M category was intermediate between SINF and all the other air mass categories. REF, CON, and HO3 generally had an average of PVU ≤ 2 except for the REF profile above 9 km where it increased to PVU ~5 at 14 km. The explanation for this increase could be that the reference air in the upper troposphere could be a mixture of low O_3 air from an upwind convective outflow with some stratospheric air that would bring the average O_3 within the ±20% limits of the reference air O_3 discriminator. For example, a mixing of seven parts of convective outflow air with O_3 = 17 ppbv and PVU = 2 with one part of stratospheric air with O_3 = 105 ppbv and PVU = 25 would produce air falling into the reference air category with O_3 = 28 ppbv and PVU = 4.9. Using PV as a discriminator might provide insight into this mixing process. However, since PV does not have the spatial resolution of the O_3 and aerosol measurements, this approach would be subject to even more uncertainties than the current method.

The PEM-Tropics B average O_3/PVU ratio in high PVU (15–30) air designated as SINF was found to have a value of about 4.0. Even in the few cases encountered with O_3 levels greater than 200 ppbv, the average O_3/PVU ratio was about 3.2. These results are still in reasonable agreement with the stratospheric O_3/PVU ratio of 4.2 estimated during PTA and used in the differentiation of PTB air masses involving enhanced O_3 (HO3, HO3M, and SINF). The only effect of using the slightly higher ratio in the PTB analysis might be the slight overestimation of air mass observations in the HO3M and SINF categories as a result of slightly overestimating the O_3 attributed to stratospheric air by less than about 15% at PVU values <10.

3.3.2. Chemical air mass characterization. A detailed in situ chemical characterization of each of the air mass types observed during PTB was determined from in situ measurements on the DC-8 [*Raper et al*., this issue] as the aircraft flew through the various air mass types that were remotely observed and categorized using the technique described above. This approach has been previously used by *Browell et al*. [1996a, 1996b] and *Fenn et al*. [1999] in characterizing the chemical composition of air mass types observed during airborne field experiments. During PTB the average chemical characteristics of the various air mass types were determined for flights 5–21 with flight 22 omitted from the analysis since it was heavily influenced by air from North and South America. For the NS category, altitudes up to 1.8 km were included. Data segments were identified for each flight that contributed to the chemical characterization of various air mass types, and separate encounters with the same air mass type during a flight were counted as independent samples.

3.3.2.1. NH and SH air mass chemical characteristics: Tables 1 and 2 present the average chemical compositions found for the major air mass types observed in NH and SH, respectively. This discrimination was necessary because of the different sources for the NH and SH air as discussed above. The CON category is only listed for the SH air (Table 2) since there were no clear cases of in situ sampling of this type of identified air mass during the NH flights. Tables 1 and 2 provide the mean and median values for each parameter and the number of independent cases that were included in the analysis of each air mass type.

The average altitude for the cases that went into the chemical characterization of each air mass type is shown, and these generally follow the expected altitude regions for the air mass types. Relative humidity (RH) values were calculated assuming that the mirror of the cryogenic hygrometer was either coated with water (RHW) or ice (RHI). The reason for giving both values is that supercooled water may exist below the freezing point of water, and there is no easy way to tell which case is present. In the tropical marine boundary layer (MBL) the mirror was most likely coated with water. At intermediate altitudes above the MBL the mirror could have been coated with either water or ice, and at higher altitudes the mirror was most likely coated with ice.

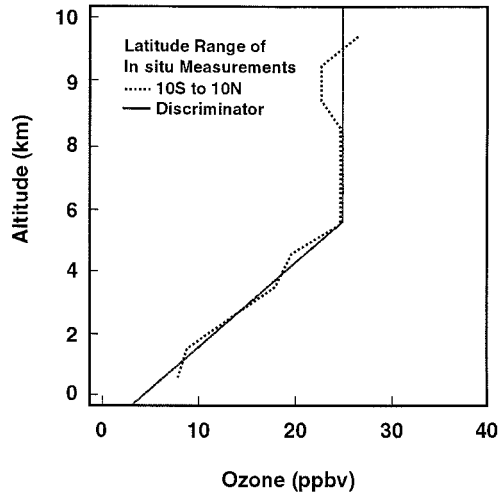

Figure 2. Average in situ O_3 profile measured over mid-Pacific during PEM-Tropics B (10°S to 10°N) and O_3 profile used as the discriminator in the air mass characterization investigation.

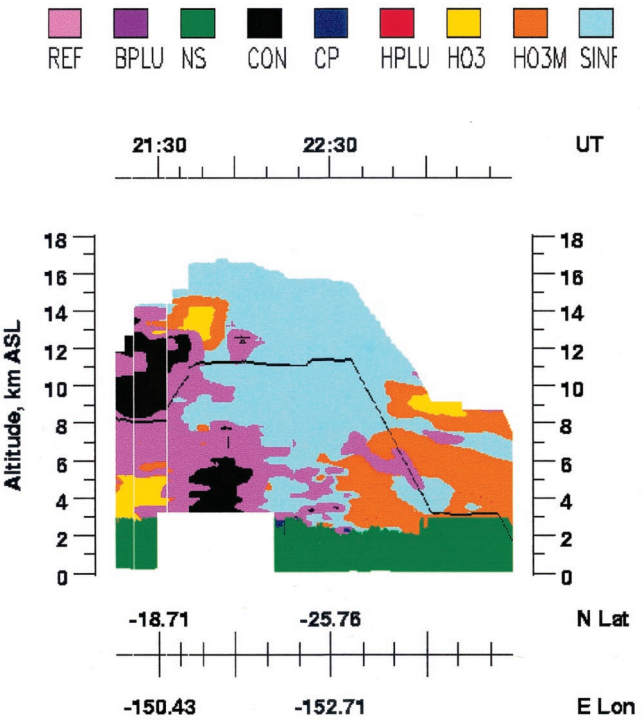

Plate 16. Example of air mass characterization based on the O_3, aerosol, and PV criteria for local Tahiti flight on April 10–11, 1999 (flight 18). The air mass types are as follows: reference (REF), background-O_3 plume (BPLU), near surface (NS), convective outflow (CON), clean Pacific (CP), high-O_3 plume (HPLU), high O_3 with low PV (HO3), high O_3 with moderate PV (HO3M), and high O_3 with high PV or stratospherically influenced air (SINF).

A number of observations can be made concerning the chemical composition observed in the various air mass types in the NH (Table 1) and SH (Table 2). The NH/SH ratios of several gases are given in Table 3 to aid in the comparison of the chemistry in the two hemispheres. All of the species listed in Table 3, with the exception of NO and NO_2 (discussed later), showed higher values in the NH compared to the SH. Ozone was about the same in REF, but it was enhanced in NH, NS, HO3, and HO3M categories. Carbon monoxide (CO) (N. S. Pougatchev et al., unpublished manuscript, 2001) and all of the hydrocarbons [*Blake et al.*, this issue], including formaldehyde (HCHO), were significantly higher in the NH compared to the SH. *Weller et al.* [2000] reported the meridional cross section of HCHO in the boundary layer of the Atlantic Ocean for October/November 1996, showing a peak in the tropics away from the ITCZ; however, the values reported by Weller et al. are higher than those found during PTB.

Methane, CO_2, HNO_3, and the halogens were also enhanced in the NH. This is attributed to the transport of NH air from Asia to the tropics as shown in the trajectory analyses discussed previously. Other indicators of air mass age are the ratios C_2H_2/CO and C_3H_8/C_2H_6 with smaller values being associated with longer ages. Compared to the NH air, the SH air showed lower values of these ratios which is consistent with older air and longer residency times over the Pacific in the SH. The higher O_3/CO ratios in the SH result from the significantly lower levels of CO with only a modest reduction in O_3.

Compared to the SH, the NO and NO_2 (S. T. Sandholm, private communication, 2001) in NS and HO3 air was slightly lower in the NH, which was possibly related to less convection and lightning in the NH [*Talbot et al.*, this issue]. There did not appear to be a trend in OH or HO_2 (Brune et al., manuscript in preparation, 2001) between the NH and SH air; however, these species, like NO, have large diurnal concentration variations [*Mauldin et al.*, 1998]. While no adjustment was made for time of the measurements, most of the flights occurred during daylight hours, generally during midday, so that the values for different air masses can be compared, albeit with some uncertainty due to the diurnal variations.

Methyl bromide (CH_3Br), derived from industrial, biomass burning, and oceanic sources [*Yokouchi et al.*, 2000a], was found to be more abundant in the NH than in the SH. *Yokouchi et al.* [2000b] found a NH/SH ratio of 1.2–1.3 from December 1996 to December 1997. The NH/SH ratio found during PTB for several air masses was about 1.1. However, the values determined for the two hemispheres include significant contributions from the tropics, the primary source region identified by Yokouchi et al. Another way to determine the NH/SH ratio is to use regions only poleward of the ITCZ and SPCZ, as done by *Avery et al.* [this issue].

Methyl iodide (CH_3I) is relatively abundant in the marine boundary layer since the ocean is its source, and thus might serve as a tracer of marine convection [*Davis et al.*, 1996; *Cohan et al.*, 1999]. As shown in Table 2, the average CH_3I value was highest in the NS and CON air masses. The composition of CON was similar to the composition of NS, except for exhibiting much lower levels of H_2O_2, which is removed in cloud convective processes, and for having much higher ultrafine and unheated aerosol number densities, which may be associated with aerosol formation processes in cloud outflow regions.

Other authors [*Avery et al.*, this issue; *Blake et al.*, this issue] did not separate their chemical characterization by air mass types, but binned their air mass characteristics in broad altitude and geographic regions relative to the ITCZ and SPCZ. Thus the values reported in Tables 1 and 2 cannot be com-

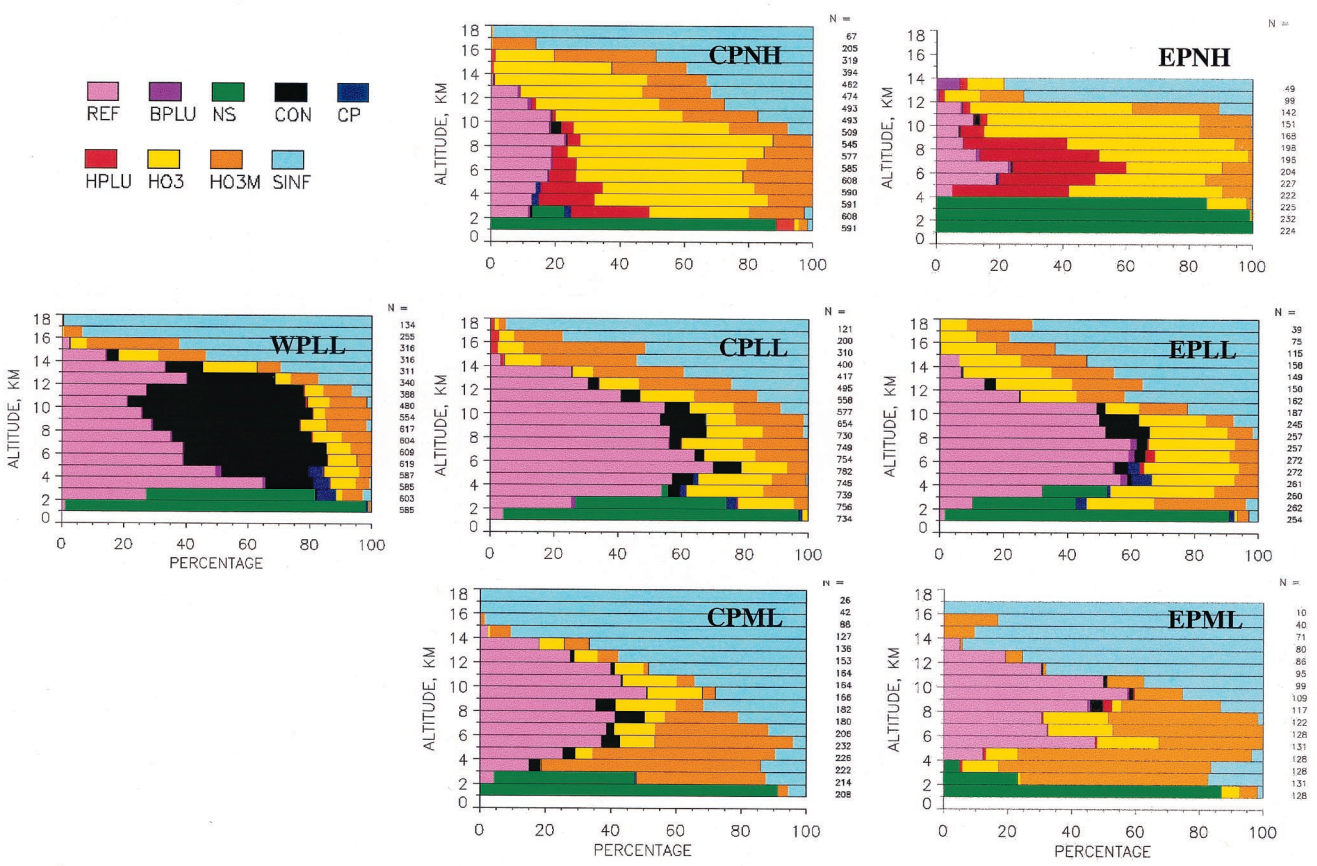

Plate 17. Percentage of time air mass categories were observed as a function of altitude in the various regions over the Pacific (see Figure 1).

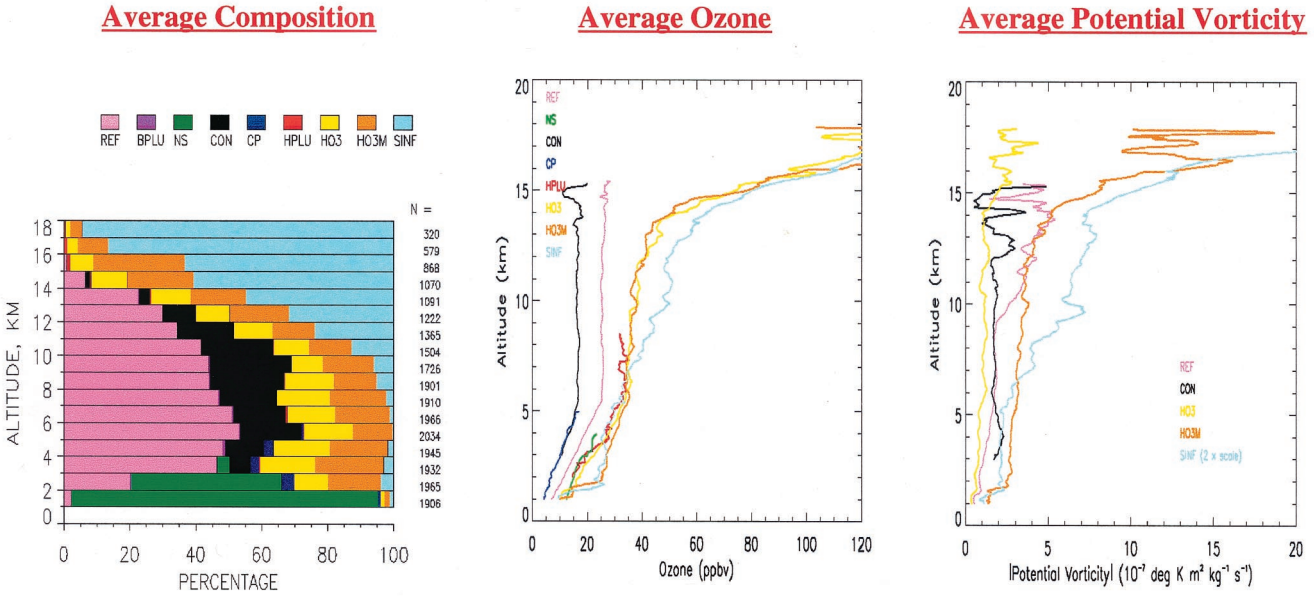

Plate 18. Average percentage of time SH air masses (<5°N) were observed at different altitudes and average O_3 and PV profiles for each of the major air mass categories. Note that PV scale for SINF is twice that for the other air mass types.

pared directly to the results of *Avery et al*. [this issue] and *Blake et al*. [this issue].

3.3.2.2. Comparison of PTB and PTA air mass chemical characteristics: A number of observations can be made in comparing the PTB SH air mass compositions with those determined during PTA [*Fenn et al*., 1999; *Singh et al*., 2000]. Biomass burning was very much in evidence in the SH during PTA but largely absent during PTB. CO and most of the nonmethane hydrocarbons (C_2H_2, C_2H_6, and C_3H_8) were significantly lower during the low biomass burning period of PTB [*Blake et al*., this issue]. Several of the nitrogen species (NO_2, HNO_3, PAN, and NO_3^-) are associated with biomass burning, and they were generally lower during PTB than PTA. Ozone was significantly lower during PTB in all air mass types, and this is associated with a general reduction in photochemical production of O_3 in the SH. Other species, such as CH_4 and CO_2, were higher in all air mass types, and this is thought to be associated with the different seasonal background levels.

Aerosol concentrations (UFA and FAU) were several times higher during PTB than during PTA. At least one aerosol precursor, SO_2, was considerably more abundant in PTB than in PTA. The category ultrafine aerosol (UFA) includes aerosols with radii >8 nm, while the category fine aerosol unheated (FAU) includes aerosols with radii >18 nm. Since aerosols often form by nucleation and grow with time, the ratio FAU/UFA is correlated with age of the aerosols, with a smaller ratio being associated with shorter ages, that is, a smaller fraction of larger particles. The characteristic times for growth from 8–18 nm to >18 nm appear to be minutes to an hour or so [*Hoppel et al*., 1994]. If aerosols are still nucleating, the ratio will reflect that fact by being low. The ratios observed during PTB were only slightly higher than those observed during PTA, indicating that the short-term age of the air, in terms of aerosol formation, was not too different in the two missions.

Another indicator of air mass age is the ratio of C_2H_2 to CO, with smaller values being associated with longer ages. C_2H_2 has a lifetime of 0.041 years (15 days) [*Ehhalt et al*., 1998], which is much longer than aerosol growth rates. The PTB SH values were found to be significantly lower than the PTA values. The values (mean/median) for REF were 0.32/0.33 and 0.81/0.78 for PTB and PTA, respectively, 0.41/0.37 versus 1.09/1.13 for HO3M and 0.44 versus 1.14/1.15 for HO3. These values indicate that the air masses sampled during PTB were considerably older than those observed during PTA.

Long-lived species are better mixed and have much less spatial or temporal variation than short-lived species. Thus CH_3Cl, with a lifetime of 1.26 years, has less variation than do CH_3Br (0.8 years), C_2Cl_4 (0.27 years), and C_2H_6 (0.18 years) [*Coleman et al*., 1998]. The standard deviations for these species for 23 cases in the REF air mass, expressed as a fraction of the mean concentration, were 0.025, 0.061, 0.404, and 0.312, respectively, in general agreement with *Coleman et al*. [1998].

Long-lived greenhouse gas concentrations rose between PTA and PTB: REF air levels of CH_4 rose from 1704.6/1704.4 ppbv to 1720.2/1719.8 ppbv in the SH, and CO_2 rose from 360.9/361.0 ppmv to 366.7/366.7 ppmv. Similar results were found between PEM-West A (September/October 1991) [*Browell et al*., 1996a] and PTB in the NH: BKG (REF) CH_4 during PEM-West-A averaged 1723.9 ppbv, while REF CH_4 during PTB in the NH was 1738.5 ppbv. An accurate comparison of values between periods should also consider the season of the measurement. The apparently slow rate of growth of CH_4 appears to continue a trend noted by *Dlugokencky et al*. [1998], who noted an average increase of 9–17% per year from 1984–1991 and −1% to 8% per year from 1992–1996.

4. Summary and Conclusions

The PTB field experiment provided the first large-scale characterization of air masses over the remote tropical Pacific Ocean during the austral late summer to early fall. The simultaneous UV DIAL- and LASE-derived measurements of O_3, H_2O, aerosols, and clouds across the troposphere along the flight track of the DC-8 aircraft allowed a more complete investigation of this area than ever before. PTB was conducted during a period of minimal biomass burning in the SH, and current results provide an important contrast to those of PTA which was conducted in the austral late winter to early spring when biomass burning was widespread in the SH. During PTB there was considerably less O_3 than observed during the SH biomass burning period of PTA. The air mass characterization for PTA showed a large incidence in the high O_3 (HO3) category (>60%) in the lower troposphere of central Pacific low latitudes compared to less than 24% in PTB. The enhanced O_3 during PTA was a direct result of long-range transport of photochemically produced O_3 from Africa and possibly as far away as Brazil.

The reduced O_3 air observed during PTB was primarily confined to the SH tropical region from about 20°S to the ITCZ on the north and the SPCZ on the west. The moist easterly flow across the Pacific in the SH tropical region experienced progressive chemical O_3 loss as it traveled to the western Pacific where O_3 was found to be the lowest throughout the troposphere from less than 10 ppbv near the surface to less than 20 ppbv at 12 km. Ozone was generally negatively correlated with H_2O across the Pacific with SH tropical air having generally less O_3 and more H_2O compared to NH air north of the ITCZ and SH subtropical air south of the SPCZ or ~20°S. NH air had more cases of enhanced aerosols in plumes in the free troposphere than the SH air. The Asian/North American origins of the NH air and the Australian/African origins of the SH subtropical air were in contrast to the relatively slow easterly flow of SH tropical Pacific air that has not had continental influences from South America/Central America for many weeks. Conditions are optimum in the SH tropical Pacific air for photochemical loss of O_3 (no continental pollution sources, high H_2O, and high solar insolation), and this is reflected in its average O_3 profile with 12 ppbv at 1 km to about 28 ppbv from 7 to above 11 km.

Westerly flow in the middle and upper troposphere was stronger in the SH during PTA than PTB, and there was extensive biomass burning in Africa and other countries upwind of the South Pacific. Thus the resulting influence of biomass burning sources on the remote tropical Pacific was much greater during PTA. A comparison of the average latitudinal and longitudinal O_3 distributions for PEM-Tropics A and B provides clear evidence of the differences in flow conditions and chemistry between the two seasons. The latitudinal and longitudinal variations of the tropopause level can also be seen in the O_3 distributions for the two missions. More stratospheric intrusions were observed during PTA than PTB; however, in both seasons, intrusions were found to extend to low latitudes (~20°S) in some cases. The observed intrusions in both field experiments contributed to determining the latitudinal structure of the tropopause and the O_3 budget in the upper troposphere in the subtropics.

Air mass characteristics were determined for seven regions over the Pacific. Nine air mass types were identified for PTB based on their O_3, aerosols, clouds, and PV characteristics. Data from each flight were categorized for each identified air mass, and these results were binned with altitude in the seven regions. NH air over the central and eastern Pacific had significantly different properties than SH air south of the ITCZ. The majority of the air masses in the NH were associated with O_3-enhanced air in aerosol plumes or in low-aerosol air not associated with stratospheric intrusions. This is consistent with the 10-day back trajectories that originate over Asia. The SH low latitudes have mostly low O_3 levels associated with reference or background air and even lower O_3 associated with convective outflow and very low "clean Pacific" air. In midlatitudes the stratospheric influence is greater with more intrusions and the associated irreversible mixing of a portion of the stratospheric air into the troposphere. The altitude dependence of this observed process was also determined. The average composition for midtropospheric SH air was found to be dominated by the reference air (45–50%) which has a low O_3 profile ($\leq$28 ppbv) to 15 km. Convective outflow of very low O_3 air from the surface, air with enhanced O_3 due to photochemistry, and air with enhanced O_3 due to a combination of photochemistry and stratospheric influences were found to be in comparable amounts (15–20% each) across this same region. Average O_3 and PV profiles for each of the dominant air mass types were discussed with respect to their contribution to the observed chemical composition of SH air over the tropical Pacific, and an average O_3/PVU ratio of about 4.0 was found in stratospheric air near the tropopause in good agreement with PTA observations.

Major differences were observed in the chemical composition of the NH and SH air mass types with the NH air in the tropics being dominated by continental pollution transported from Asia. The air in the SH tropics had lower O_3, CO, hydrocarbons, PAN, HNO_3, and halocarbons compared to the NH air, and this air had lower C_2H_2/CO and C_3H_8/C_2H_6 ratios indicating older air. Composition of SH convective outflow air (CON) was similar to the near-surface (NS) air without the soluble species, but CON also had very elevated aerosol concentrations (UFA and FAU) which indicated considerable aerosol formation in the outflow regions.

Biomass burning influences on SH air during PTA dominated the chemical differences between PTA and PTB. PTB had greatly reduced O_3, CO, hydrocarbons, PAN, HNO_3, and nitrate due to low burning influences, but enhanced CH_4, CO_2, CH_3I, and fine aerosols due to long-term trends and seasonal cycles. The SH air during PTB was considerably older in all air mass categories than the PTA air, and while the O_3 was lower during PTB, the CO levels were even lower so that the O_3/CO ratio was significantly lower for all the free tropospheric air mass types (REF, HO3, HO3M, and CON). The near surface (NS) category had nearly the same ratio as for PTA indicating that much of the impact of the PTA biomass burning was limited to the free troposphere. During PTB the average median O_3/CO ratio of 0.35 in the near-surface (NS) air was found to be nearly the same as that found in the convective outflow air (CON) of 0.33, and this demonstrates the direct transport of air from near the surface to the mid to upper troposphere in cloud convective events.

Acknowledgments. The authors thank Ben Barker, Chris Edwards, Shlomo Fastig, Dave Harper, Lorraine Heilman, George Insley, George Lockard, Leroy Matthews, Bill McCabe, Tony Notari, Loyd Overbay, Larry Petway, and Jerry Williams at the NASA Langley Research Center for their assistance in all aspects related to installing, operating, and maintaining the airborne UV DIAL and LASE systems on the DC-8 during the PTB field experiment and in postmission data reduction and analyses tasks. We appreciate the cooperation of the NASA Dryden Flight Research Center's DC-8 flight crew in conducting this field experiment. The funding for this investigation came from the NASA Tropospheric Chemistry Program, and the MTP work performed by M. J. Mahoney was carried out by the Jet Propulsion Laboratory, California Institute of Technology, under a contract with NASA.

References

Avery, M. A., D. J. Westberg, H. E. Fuelberg, R. E. Newell, B. Anderson, S. A. Vay, G. W. Sachse, and D. R. Blake, Chemical transport across the ITCZ in the central Pacific during an El Niño Southern Oscillation cold phase event in March–April 1999, *J. Geophys. Res*., this issue.

Blake, N. J., et al., Large-scale latitudinal and vertical distributions of NMHCs and selected halocarbons in the troposphere over the tropical Pacific Ocean during the March–April 1999 Pacific Exploratory Mission (PEM-Tropics B), *J. Geophys. Res*., this issue.

Browell, E. V., Remote sensing of tropospheric gases and aerosols with an airborne DIAL system, in *Optical Laser Remote Sensing*, edited by D. K. Killinger and A. Mooradian, pp. 138–147, Springer-Verlag, New York, 1983.

Browell, E. V., Differential absorption lidar sensing of ozone, *Proc. IEEE*, *77*, 419–432, 1989.

Browell, E., and S. Ismail, First lidar measurements of water vapor and aerosols from a high-altitude aircraft, paper presented at Symposium on Optical Remote Sensing of the Atmosphere, Opt. Soc. of Am., Salt Lake City, Utah, Feb. 5–9, 1995.

Browell, E. V., A. F. Carter, S. T. Shipley, R. J. Allen, C. F. Butler, M. N. Mayo, J. H. Siviter Jr., and W. M. Hall, NASA multipurpose airborne DIAL system and measurements of ozone and aerosol profiles, *Appl. Opt*., *22*, 522–534, 1983.

Browell, E. V., S. Ismail, and S. T. Shipley, Ultraviolet DIAL measurements of O_3 profiles in regions of spatially inhomogeneous aerosols, *Appl. Opt*., *24*, 2827–2836, 1985.

Browell, E. V., C. F. Butler, S. A. Kooi, M. A. Fenn, R. C. Harriss, and G. L. Gregory, Large-scale variability of ozone and aerosols in the summertime Arctic and subarctic troposphere, *J. Geophys. Res*., *97*, 16,433–16,450, 1992.

Browell, E. V., et al., Large-scale air mass characteristics observed over the western Pacific during summertime, *J. Geophys. Res*., *101*, 1691–1712, 1996a.

Browell, E. V., et al., Ozone and aerosol distributions and air mass characteristics over the South Atlantic Basin during the burning season, *J. Geophys. Res*., *101*, 24,043–24,068, 1996b.

Browell, E. V., et al., LASE validation experiment, in *Advances in Atmospheric Remote Sensing With Lidar*, edited by A. Ansmann et al., pp. 289–295, Springer-Verlag, New York, 1997.

Browell, E. V., S. Ismail, and W. B. Grant, Differential Absorption Lidar (DIAL) measurements from air and space, *Appl. Phys. B*., *67*, 399–410, 1998.

Browell, E. V., S. Ismail, and R. Ferrare, Hurricane water vapor, aerosol, and cloud distributions determined from airborne lidar measurements, paper presented at Symposium on Lidar Atmospheric Monitoring, Am. Meteorol. Soc., Long Beach, Calif., Jan. 9–14, 2000.

Cohan, D. S., M. G. Schultz, D. J. Jacob, B. G. Heikes, and D. R. Blake, Convective injection and photochemical decay of peroxides in the tropical upper troposphere: Methyl iodide as a tracer of marine convection, *J. Geophys. Res*., *104*, 5717–5724, 1999.

Coleman, J. J., D. R. Blake, and F. S. Rowland, Atmospheric residence time of CH_3Br estimated from the Junge variability relation, *Science*, *281*, 392–396, 1998.

Davis, D., J. Crawford, S. Liu, S. McKeen, A. Bandy, D. Thornton, F. Rowland, and D. Blake, Potential impact of iodine on tropospheric levels of ozone and other critical oxidants, *J. Geophys. Res*., *101*, 2135–2147, 1996.

Dlugokencky, E. J., K. A. Masarie, P. M. Lang, and P. P. Tans, Continuing decline in the growth rate of the atmospheric methane burden, *Nature*, *393*, 447–450, 1998.

Ehhalt, D. H., F. Rohrer, A. Wahner, M. J. Prather, and D. R. Blake, On the use of hydrocarbons for the determination of tropospheric OH concentrations, *J. Geophys. Res*., *103*, 18,981–18,997, 1998.

Fenn, M. A., E. V. Browell, and C. F. Butler, Airborne lidar measurements of ozone and aerosols during PEM-West A and PEM-West B, in *Advances in Atmospheric Remote Sensing With Lidar*, edited by A. Ansmann et al., pp. 355–358, Springer-Verlag, New York, 1997.

Fenn, M. A., et al., Ozone and aerosol distributions and air mass characteristics over the South Pacific during the burning season, *J. Geophys. Res*., *104*, 16,197–16,212, 1999.

Ferrare, R., et al., LASE measurements of water vapor, aerosols, and clouds during CAMEX-3, paper presented at Symposium on Optical Remote Sensing of the Atmosphere, Opt. Soc. of Am., Santa Barbara, Calif., 1999.

Ferrare, R., et al., Comparison of aerosol optical properties and water vapor among ground and airborne lidars and Sun photometers during TARFOX, *J. Geophys. Res*., *105*, 9917–9933, 2000a.

Ferrare, R., et al., Comparisons of LASE, aircraft, and satellite measurements of aerosol optical properties and water vapor during TARFOX, *J. Geophys. Res*., *105*, 9935–9947, 2000b.

Fishman, J., V. G. Brackett, E. V. Browell, and W. B. Grant, Tropospheric ozone derived from TOMS/SBUV measurements during TRACE-A, *J. Geophys. Res*., *101*, 24,069–24,082, 1996.

Fuelberg, H. E., R. E. Newell, S. P. Longmore, Y. Zhu, D. J. Westberg, E. V. Browell, D. R. Blake, G. L. Gregory, and G. W. Sachse, A meteorological overview of the Pacific Exploratory Mission (PEM) Tropics period, *J. Geophys. Res*., *104*, 5585–5622, 1999.

Fuelberg, H. E., R. E. Newell, D. J. Westberg, J. C. Mahoney, J. R. Hannan, B. C. Martin, and Y. Zhu, A meteorological overview of the Second Pacific Exploratory Mission in the Tropics, *J. Geophys. Res*., this issue.

Hoell, J. M., D. D. Davis, D. J. Jacob, M. O. Rodgers, R. E. Newell, H. E. Fuelberg, R. J. McNeal, J. L. Raper, and R. J. Bendura, Pacific Exploratory Mission in the tropical Pacific: PEM-Tropics A, August–September 1996, *J. Geophys. Res*., *104*, 5567–5583, 1999.

Hoppel, W. A., G. M. Frick, J. W. Fitzgerald, and R. E. Larson, Marine boundary layer measurements of new particle formation and the effects nonprecipitating clouds have on aerosol size distribution, *J. Geophys. Res*., *99*, 14,443–14,459, 1994.

Mauldin, R. L., III, G. J. Frost, G. Chen, D. J. Tanner, A. S. H. Prevot, D. D. Davis, and F. L. Eisele, OH measurements during the First Aerosol Characterization Experiment (ACE 1): Observations and model comparisons, *J. Geophys. Res*., *103*, 16,713–16,729, 1998.

Moore, A. S., Jr., et al., Development of the Lidar Atmospheric Sensing Experiment (LASE)—An advanced airborne DIAL instrument, in *Advances in Atmospheric Remote Sensing With Lidar*, edited by A. Ansmann et al., pp. 281–288, Springer-Verlag, New York, 1997.

Newell, R. E., and M. J. Evans, Seasonal changes in pollutant transport to the North Pacific: The relative importance of Asian and European sources, *Geophys. Res. Lett*., *27*, 2509–2512, 2000.

Olson, J. R., B. A. Baum, D. R. Cahoon, and J. H. Crawford, Frequency and distribution of forest, savanna, and crop fires over tropical regions during PEM-Tropics A, *J. Geophys. Res*., *104*, 5865–5876, 1999.

Oltmans, S. J., et al., Ozone in the Pacific tropical troposphere from ozonesonde observations, *J. Geophys. Res*., this issue.

Raper, J. L., M. M. Kleb, D. J. Jacob, D. D. Davis, R. E. Newell, H. E. Fuelberg, R. J. Bendura, J. M. Hoell, and R. J. McNeal, Pacific Exploratory Mission in the tropical Pacific: PEM-Tropics B, March–April 1999, *J. Geophys. Res*., this issue.

Richter, D. A., E. V. Browell, C. F. Butler, and N. S. Higdon, Advanced airborne UV DIAL system for stratospheric and tropospheric ozone and aerosol measurements, in *Advances in Atmospheric Remote Sensing With Lidar*, edited by A. Ansmann et al., pp. 395–398, Springer-Verlag, New York, 1997.

Sasano, Y., and E. V. Browell, Light scattering characteristics of various aerosol types: Multiple wavelength lidar observations, *Appl. Opt*., *28*, 1670–1679, 1989.

Schultz, M. G., et al., On the origin of tropospheric ozone and NO_x over the tropical South Pacific, *J. Geophys. Res*., *104*, 5829–5843, 1999.

Singh, H. B., et al., Biomass burning influences on the composition of the remote South Pacific troposphere: Analysis based on observations from PEM-Tropics A, *Atmos. Environ*., *34*, 635–644, 2000.

Talbot, R. W., et al., Influence of biomass combustion emissions on the distribution of acidic trace gases over the southern Pacific basin during austral springtime, *J. Geophys. Res*., *104*, 5623–5634, 1999.

Weller, R., O. Schrems, A. Boddenberg, S. Gab, and M. Gautrois, Meridional distribution of hydroperoxides and formaldehyde in the marine boundary layer of the Atlantic (48°N–35°S) measured during the Albatross campaign, *J. Geophys. Res*., *105*, 14,401–14,412, 2000.

Yokouchi, Y., et al., A strong source of methyl chloride to the atmosphere from tropical coastal land, *Nature*, *403*, 295–298, 2000a.

Yokouchi, Y., et al., Latitudinal distribution of atmospheric methyl bromide: Measurements and modeling, *Geophys. Res. Lett*., *27*, 697–700, 2000b.

B. E. Anderson, M. A. Avery, J. D. W. Barrick, V. G. Brackett, E. V. Browell, C. F. Butler, M. B. Clayton, M. A. Fenn, R. A. Ferrare, W. B. Grant, S. Ismail, S. A. Kooi, and G. W. Sachse, Atmospheric Sciences, NASA Langley Research Center, MS-401A, Hampton, VA 23681. (e.v.browell@larc.nasa.gov)

D. R. Blake, Department of Chemistry, University of California, Irvine, CA 92717.

W. H. Brune, Department of Meteorology, Pennsylvania State University, University Park, PA 16802.

H. E. Fuelberg and J. C. Maloney, Department of Meteorology, Florida State University, Tallahassee, FL 32306.

B. G. Heikes, Graduate School of Oceanography, University of Rhode Island, Narragansett, RI 02882.

M. J. Mahoney, Jet Propulsion Laboratory, California Institute of Technology, Pasadena, CA 91125.

R. E. Newell and Y. Zhu, Department of Earth, Atmospheric, and Planetary Sciences, Massachusetts Institute of Technology, Cambridge, MA 02139.

H. B. Singh, NASA Ames Research Center, Moffett Field, CA 94035.

R. W. Talbot, Institute for the Study of Earth, Oceans, and Space, University of New Hampshire, Durham, NH 03824.

(Received September 7, 2000; revised December 20, 2000;
accepted January 3, 2001.)